applied sciences

MDPI

Article

Multidiscipline Design Optimization for Large-Scale Complex Nonlinear Dynamic System Based on Weak Coupling Interfaces

Wei Du [1,2], Si-Yang Piao [3], Ming-Wei Piao [1,*], Chun-Ge Nie [3], Peng Dang [4], Qiu-Ze Li [4] and Yi-Nan Tao [1]

[1] Mechanical Engineering School, Dalian Jiaotong University, Dalian 116028, China
[2] Railway Rolling Stock College, Liaoning Railway Vocational and Technical College, Jinzhou 121000, China
[3] Locomotive and Rolling Stock Engineering College, Dalian Jiaotong University, Dalian 116028, China
[4] CRRC Changchun Railway Vehicles Co., Ltd., Changchun 130062, China
* Correspondence: m_w_piao@126.com

Abstract: For high-tech manufacturing industries, developing large-scale complex nonlinear dynamic systems must be taken as one of the basic works, formulating problems to be solved, steering system design in a more preferable direction, and making correct strategic decisions. By using effective tools of big data mining, Dynamic Design Methodology was proposed to establish a technical platform for Multidiscipline Design Optimization such as High-Speed Rolling Stock, including three key technologies: analysis graph of full-vehicle stability properties and variation patterns, improved transaction strategy of flexible body to MBS interface, seamless collaboration with weldline fatigue damage assessments through correct Modal Stress Recovery. By applying the above methodology, a self-adaptive improved solution was formulated with optimal parameter configuration, which is one of the more favorable options for higher-speed bogies. While within a velocity (140–200) km/h at $\lambda_e < 0.10$, car body instability's influence on ride comfort can be easily improved by using a semi-active vibration reduction technique between inter-vehicles through outer windshields. Comprehensive evaluations show that only under rational conditions of wheel-rail matching, i.e., $0.10 \geq \lambda_{eN} > \lambda_{emin}$ and λ_{emin} = (0.03–0.06), can this low-cost solution achieve the three goals of low track conicity, optimal route planning, and investment benefit maximization. So, rail vehicle experts are necessary to collaborate and innovate intensively with passenger transportation and steel rail ones. Specifically, by adopting rail grinding treatment, occurrence probability is controlled at 85% and 5% for track conicity of (0.03–0.10) and (0.25–0.35). By optimizing routing planning, operating across dedicated lines of different speed grades can achieve self-cleaning of central hollow tread wear over time. According to the inherent rigid-flex coupling relationship, geometric nonlinearities of worn wheel-rail contact should be avoided as much as possible for HSR practices. Only under weak coupling interfaces in the floor frame can the structural integrity of an aluminum alloy car body be ensured.

Keywords: large-scale complex nonlinear dynamic system; multidiscipline design optimization; weak coupling interface; rigid-flex coupling simulation technique; modal stress recovery

check for updates

Citation: Du, W.; Piao, S.-Y.; Piao, M.-W.; Nie, C.-G.; Dang, P.; Li, Q.-Z.; Tao, Y.-N. Multidiscipline Design Optimization for Large-Scale Complex Nonlinear Dynamic System Based on Weak Coupling Interfaces. *Appl. Sci.* **2023**, *13*, 5532. https://doi.org/10.3390/app13095532

Academic Editor: Giovanni Bernardini

Received: 20 March 2023
Revised: 23 April 2023
Accepted: 26 April 2023
Published: 29 April 2023

Copyright: © 2023 by the authors. Licensee MDPI, Basel, Switzerland. This article is an open access article distributed under the terms and conditions of the Creative Commons Attribution (CC BY) license (https://creativecommons.org/licenses/by/4.0/).

1. Introduction

As for high-tech manufacturing industries such as HSRS (High Speed Rail Stock), the dynamic design methodology should be actively recommended and introduced to better develop the corresponding large-scale complex nonlinear dynamic systems. Furthermore, by applying efficient tools such as PODA (Proper Orthogonal Decomposition Approach) or MMRT (Modal Modification Responding Technique), weak coupling interfaces are necessary to be constructed between different disciplines, by which the large-scale MDO (Multidiscipline Design Optimization) technical platform can be established, steering the system design in a more preferable direction.

The large-scale complex nonlinear dynamic systems usually have two classes of nonlinear influences, i.e., non-smooth and large displacement, and three kinds of nonlinear

vibration behaviors, i.e., parametric disturbance, self-excited oscillation, and forced vibration. Taking HSRS for instance, the dynamics equations of MBS (Multi-Body System) are comprised of the (non-) holonomic constraints, i.e., $\boldsymbol{C} = \boldsymbol{C}_1 \cup \boldsymbol{C}_2$, and index-3 DAEs (Differential Algebraic Equations) as follows [1,2]:

$$\boldsymbol{M}\ddot{q} + \boldsymbol{C}_q^T \lambda = \boldsymbol{Q} \tag{1}$$

where $\boldsymbol{M}$ is the mass matrix, asymmetric and not positive definite due to the redundant constraints, which cannot be then inversed; $\boldsymbol{Q}$ is the total external force, including the non-conservative forces; λ is the undetermined factor, which is combined with the transposition of the following matrix (2) to constitute the inner force term, including the Coriolis force.

$$\boldsymbol{C}_q \equiv: \frac{\partial \boldsymbol{C}}{\partial q} \tag{2}$$

However, the generalized space variable $\boldsymbol{q}$ must satisfy the following constraints:

Holonomic constraints $\boldsymbol{C}_1 = 0, \dot{\boldsymbol{C}}_1 = 0$ *and* $\ddot{\boldsymbol{C}}_1 = 0$

Non-holonomic constraints $\boldsymbol{C}_2 = 0$ *and* $\dot{\boldsymbol{C}}_2 = 0$.

Therefore, $\boldsymbol{q}$ can be further divided into two subsets: independent variables and dependent variables, i.e., $q = y \cup x$.

Generally, the SSR (State Space Reduction) method needs to meet the following conditions

$$\det(\boldsymbol{C}_x) \neq 0 \text{ (Non-singularity)} \tag{3}$$

But the integral algorithm of improved augmentation proposed by Negrut [1] can deal with this difficult problem successfully. Taking velocity and acceleration as basic variables and their derivatives and applying Newmark's second-order difference technique, this kind of improved generalized augmented algorithm can further condense the Jacobian matrix and reduce the occurrence probability of ill-condition, thus achieving the accurate analysis results of complex constrained inner forces [2]. Although the calculation is complicated and inefficient, the above variable-step integration algorithm has been sufficiently validated for solving dynamic engineering problems under the technical support of better hardware and software platforms.

Unlike the situations of launch or road vehicles [3], the variable-step integration algorithm can be regarded as one of the most effective tools to promote the development of modern rail vehicle system dynamics. The duality of hunting kinematics and dynamics is the essence or basic problem of rail vehicle system dynamics [4,5]. The hunting motion stabilization can only be achieved under the rational condition of wheel-rail matching, i.e., the hypothesis of small creepage and non-spin is valid when the actual equivalent conicity $\lambda_e < 0.10$, resulting in the low dynamic interactions of wheel-rail contact, which is also referred to as the first weak coupling interface. For this reason, the so-called "frozen mode characteristics" are introduced under the mechanism of large damping to suppress hunting. Specifically, although the corresponding poles are very close to the imaginary axis, the time constant is very large, and the transient time to steady state behavior is also very large under this large damping mechanism, i.e., apparently a steady state of sinusoidal oscillations takes place.

Nevertheless, the hunting motion stabilization is not unconditional, nor is it necessary to implement the so-called quasi-static perturbation simulations and then carry out the multidisciplinary collaborative simulations on the basis of synchronous data exchange [6,7]. With regard to the non-smooth nonlinear impacts that occurred on rail vehicle system dynamics, True first raised an objection to the equal-step integration algorithm [8]. Under the rigorous service conditions of high-speed operation on dedicated lines, e.g., the longer the nose of the car head's streamlined design at both ends, the stronger the aerodynamic loads caused by the wake disturbances [9]. As a result, the hollow wear on wheel tread is accompanied by the eccentric wear of the wheelset, which forced the period of wheelset

re-profiling under the floor to be shortened, ca. 20×10^4 km. Too many times of wheelset re-profiling under the floor will cause dynamic imbalance [10]. Considering the improper use of anti-roll torsion bar devices existing in CRH2C improved bogies, the hollow wear on wheel tread becomes more severe [11], and the wheelset re-profiling period is further shortened to less than 10×10^4 km. In this way, the dynamic imbalance of wheelset will force the service car body to produce the first vertical bending modal vibration through the mono-bar traction devices, as shown in Figure 1a, i.e., the so-called longitudinal and vertical coupling resonance [12].

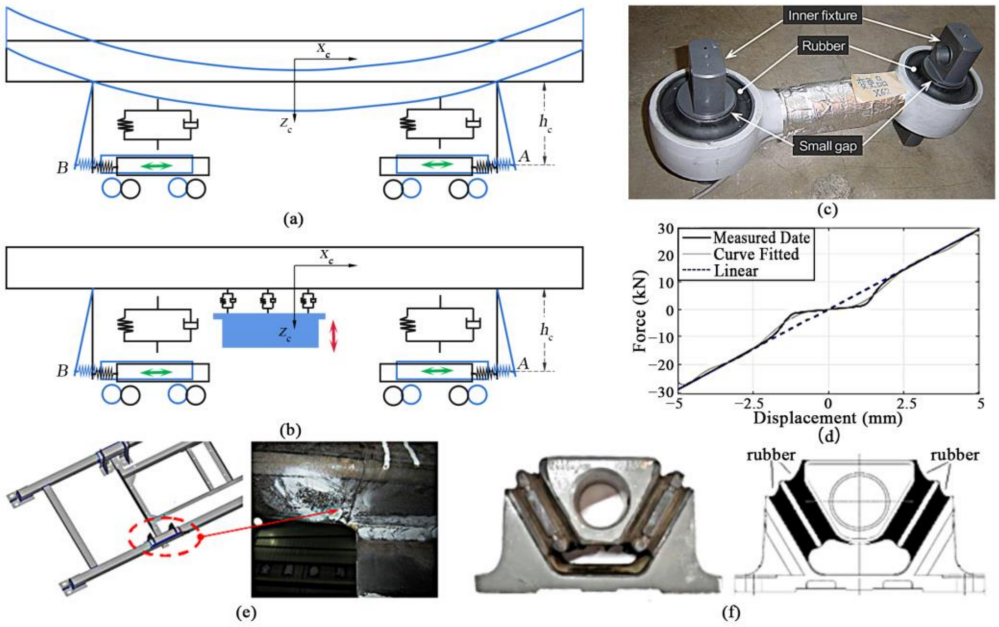

Figure 1. Longitudinal and vertical coupling relationship between running gear and service car body formulated by a mono-bar traction device under influences of wheelset dynamic imbalance. (**a**) Longitudinal and vertical coupling relationship formulated by mono-bar traction device when the service car body is regarded as a slender beam. (**b**) Reciprocating longitudinal oscillations of front and rear bogies force traction converter in the equipment cabin under floor frame to occasionally produce vertical coupling resonance. (**c**) Mono-bar traction device. (**d**) Traction stiffness curve, equivalent stiffness of which is ca. (8.0–8.5) MN/m per bogie. (**e**) Traction converter installation hanging frame was cracked thereby. (**f**) DVA damping technique is implemented incorrectly by using rubber hanging elements, and strong coupling interface to floor frame is then formed.

In order to improve the vibration comfort, as shown in Figure 1b–e, the nonlinear restraint measures of rubber joints at both ends of mono-bar traction devices proposed in the literature [13,14] are actually adopted. However, this measure is totally impractical, which caused the vertical coupling resonance of traction converter and led to the hanging frame cracking. In short, the dynamic imbalances caused by frequent wheelset re-profiling under the floor force the front and rear bogies to produce the reciprocating longitudinal oscillation in opposite and backward directions, which approaches the vertical hanging modal frequency of the traction converter. Moreover, the rubber hanging elements, as shown in Figure 1f, are misused to constitute the DVA (Dynamic Vibration Absorber) techniques, which completely ignore their application premise, i.e., the narrowband vibration response characteristics.

Special attention should be paid to the fact that the above longitudinal and vertical coupling resonances belong to the dynamic behavior of unsaturated or unsteady states. The second or third active control techniques must be used to remove or eliminate the influence of such nonlinear vibrations [15]. Therefore, these DVA techniques are difficult to work in the above circumstances.

From the perspective of concurrent design principles, the pre-search and development of dynamic systems for both motor and trailer vehicles must also consider the issue of strong/weak coupling interfaces. The structural design of the service car body system must ensure the 30-year service life of the aluminum alloy car body, and the safety of ESL (Equivalent Static Load) remains an open topic.

It is assumed that the ESL sets are equivalent to the load cases specified by the industry codes or standards under some steady states or quasi-static states. The ESL sets are defined as the loads that produce the same displacements at each time step by static analysis as the ones provided by the transient analysis. The transient analysis, as shown in Equation (4), is based on the basic equations of the HSRS rigid-flex coupling system [16,17].

$$\boldsymbol{M}\ddot{\xi} + \left(\dot{\boldsymbol{M}} - \frac{1}{2}\left[\frac{\partial \boldsymbol{M}}{\partial \xi}\dot{\xi}\right]^T + \boldsymbol{D}\right)\dot{\xi} + \boldsymbol{K}\xi + f_g + \left[\frac{\partial \boldsymbol{C}}{\partial \xi}\right]^T \mu = \boldsymbol{Q} \tag{4}$$

where $\xi = [q \quad \bar{q}]^T$, spanning across the generalized and modal spaces, i.e., MBS's generalized space variables q and flexible body's elastic modal space variables $\bar{q}$. $\boldsymbol{M}$ is the mass matrix of MBS including flexible bodies (e.g., the hypothesis of nine invariants in some analysis software such as ADAMS 2005), which is non-symmetric, non-positive definite, and non-invertible; $\boldsymbol{K}$ and $\boldsymbol{D}$ are the stiffness and damping matrices of the coupling system, respectively; f_g is the gravity obtained through the gravitational potential energies of (rigid- and flex-) entities by the partial derivation of ξ; $\boldsymbol{Q}$ is the external resultant force; μ is an undetermined factor, which can form the constrained inner force term including Coriolis forces by multiplying the transposition of formula (5).

$$\boldsymbol{C}_q \equiv: \frac{\partial \boldsymbol{C}}{\partial \xi} \tag{5}$$

Applying the strong/weak duality problem of convex optimization, the literature [18,19] believes that the structural dynamic response design based on ESL is not always convergent to obtain the optimum solution. However, the weak duality holds generally. If p^* is defined as the primal solution, and d^* as the dual solution, then $d^* \leq p^*$ for the we ak duality. The quantity $p^* - d^*$ is known as the duality gap, which can be a useful criteria for convergence. Unfortunately, for the strong dual solution, there is no similar criterion to ensure convergence.

If we ignore the application premise of DVA techniques and even use the multiple DVA technical devices, a strong coupling interface will be formed between the equipment cabin and the aluminum alloy car body. Therefore, the aluminum alloy car body does not only need to be reinforced repeatedly, leading to exceed the empty axle load limit, but also causes the equipment cabin to have bolt loosen failure or skirt bracket cracking accidents.

For this reason, the transaction strategy of flexible body to MBS interfaces is vital to the dynamic response design optimization of lightweight structures. If the couplings of flexible body to MBS interfaces are completely ignored, some analysis software [20] can only give the motion coupling relationship, completely losing the accurate analysis results of the complex constraint inner forces. For instances of two-axle freight wagons, the underframe is usually distorted and vibrated due to the roll and rock of the service car body [21]. If the rigidity of both end crossbeams is insufficient, vibration fatigue will occur between the traction beam and the end wall. Another example is that the long flat car used for the transportation of natural gas integrated tanks is reconstructed into a two-box container flat car, and the reinforcing structures are added to the longitudinal beams on both sides to reduce the deflection-span ratio. However, considering the track torsion excitations, e.g., the 25 m fixed length rails are staggered, and each rail produces ca. 20 mm static deflection because of the track bed settlements caused by groundwater upwelling, the cracks take place in the above reinforced structures thereby [22], which belong to extremely low cycle fatigue failure.

For large-scale complex nonlinear dynamic systems such as HSRS, MDO should put more emphasis on the three key points of Pareto optimization, i.e., non-dominated solu-

tion, clustering division, and key minority, instead of the genetic algorithm or particle swarm algorithm themselves. Literature [23] believes that the roles of recent data mining techniques are to support: (i) Formulation of design problems; (ii) Decision making; and (iii) Design steering. Therefore, the applications of PODA and MMRT can reasonably execute the clustering division and better face the frontier of Pareto design [24–27], so as to firmly grasp the two important influencing factors of wheel-rail contact and bogie suspension. Especially, under the condition of multiple constraints [28], the large-scale MDO such as HSRS should adopt a dialectical and unified analysis viewpoint, i.e., the hunting motion stabilization is conditional, which depends mainly on the geometric nonlinearity of worn wheel-rail contact. And the self-adaptive improved bogie designs make the wheel-rail matching back to the rational condition for higher-/high-speed rails, which is one of the most important interpretations for non-dominated solution.

MDO is also the key to the commercial applications of high-tech integrating systems such as HSRS. To remove and eliminate the detrimental wear and associated negative impacts is one of the technical bottlenecks in the operation and maintenance practices of worldwide HSR (High Speed Rails). There are two technical solutions to detrimental wear as follows: one is the improved design of the wheel-rail relationship for HSR; the other is the self-adaptive improved design of higher-/high-speed bogies, and making it becomes a technical platform for MDO among vehicles, rails, passenger transport, etc. Especially, the operating mileage of Chinese rails has reached 15.3×10^4 km at present, including HSR of 4.1×10^4 km, accounting for 26.8%. For this reason, successful commercial applications of HSRS must have some key technologies to improve the associated technical economy. Therefore, the large-scale MDO such as HSRS need to use PODA and MMRT as effective tools for big data mining so as to achieve the three important goals of low track conicity, optimal routing plans, and investment benefit maximization.

Overall, for high-tech equipments such as HSRS, the development of corresponding dynamic systems must be guided the following two criteria: firstly, model reduction and simplification cannot lose the essential characteristics of engineering problems, i.e., the eigen modeling; secondly, different professions need to handle the dynamic interaction between each other's interfaces, i.e., the strong/weak coupling interface. On this basis, an MDO technology platform can be established by using big data mining methods such as PODA, MMRT, etc., so as to support the successful commercial application of high-tech equipments and achieve the above three important goals.

It should be emphasized that the longitudinal uneven wear problem of wheel-rail rolling contact is not within the scope of the investigation in this paper. Although many scholars believe that the flat scar wheel is one of the main factors related to the formation of longitudinal uneven wear, there are still diverse causes, such as the dynamic imbalance of wheelsets. The longitudinal uneven wear can cause the abnormal dynamic impacts of wheel-rail contact, involving the wave dynamics of seamless steel rails and the vibration propagation of track bed foundations.

In combination with our previous works, the aim of this research paper is to actively recommend and introduce the dynamic design methodology into high-tech manufacturing industries such as HSRS, so as to make the following three contributions to collaborative innovations among different disciplines:

(1) The analysis graph of full-vehicle stability properties and variation patterns was formulated by using PODA to clarify the correct direction of self-adaptive improvement, removing and eliminating the unfavorable convected motion relationship, and making the beneficial one more robust, by which the rational condition of wheel-rail matching can be regressed so as to obtain the uniform wear stage at low conicity.

(2) Learn from MMRT based on the boundary loading treatment [29,30], the transaction strategy was further improved for the flexible body to MBS interface so that the service car body system can realize the weak coupling design for the interface of the equipment cabin, completely removing and eliminating the lateral coupling relationship between running gear and service car body.

(3) According to the inherent rigid-flex coupling relationship of HSRS, the correctness of MSR (Modal Stress Recovery) can be ensured by the accurate analysis results of complex constrained inner forces, by which a seamless collaborative platform was established by integrating with the weldline fatigue damage assessment method based on the master S-N curve of Dong's structural stress.

For this reason, two efficient tools of PODA and MMRT will be briefly introduced in the Section 2, and the flow chart is formulated for large-scale MDO such as HSRS. Referring to the present domestic and foreign experiences and the contrastive analyses between tests and simulations, the Section 3 will further clarify the correct improved design direction of HSRS to achieve the rational condition of wheel-rail matching at the lowest cost. The Section 4 presents the self-adaptive improved solution for higher speed bogies and associated technical features, e.g., semi-active damping technique between inter-vehicles, the realization of uniform wear strategy at low conicity, and the technical feasibility of breaking the 575 km/h record in worldwide HSR practices. Finally, the main conclusions of this research are summarized in the Section 5, and future work is briefly prospected based on some findings achieved in large-scale MDO applications such as HSRS.

2. Large-Scale MDO by Using PODA and MMRT

For the development of large-scale complex nonlinear dynamic systems such as HSRS, there are two key issues that must be clearly addressed: (i) As a visual data mining tool, the analysis graph of full-vehicle stability property and variation patterns can be formulated by using PODA, and the optimal parameter configuration of higher speed bogies is determined accordingly, so as to steer the system design to the correct direction of self-adaptive improved design; (ii) Taking the boundary loading treatment as an effective method for the FEM updating, the transaction strategy for the flexible body to MBS interface can be improved by MMRT, so as to ensure the 30-year service life of aluminium alloy car body with the weak coupling interface as far as possible.

2.1. Analysis Graph of Full-Vehicle Stability Properties and Variation Patterns

The improved generalized augmented method is aimed at the singularity problem of complex constraints, using the ingenious combination of independent generalized variables and virtual augmented variables to quickly capture the perturbation direction with minimum resistance, thus forming a variable step integration algorithm with three stages of forecast, correction, and evaluation.

Assuming u and $T\dot{q} = u$, and designating $\overline{q}, \overline{u}$ as the virtual augmentation variables, we get then from Equation (1), as stated in literature [1]

$$\left.\begin{array}{c} \boldsymbol{M}\dot{u} + \boldsymbol{P}\lambda - \boldsymbol{Q} = 0 \\ \boldsymbol{B}_1 u = \overline{u} \\ \boldsymbol{B}_0 q = \overline{q} \end{array}\right\} \tag{6}$$

where $\boldsymbol{P} = \boldsymbol{P}(q)$ is a projective operator, which represents the partial differential transformation relation of (non-) holonomic constraints as shown in Formula (2). $\boldsymbol{B}_0$ and $\boldsymbol{B}_1$ are the Boolean matrices.

The Equation (6) can be rewritten as follows

$$\boldsymbol{F}(\dot{u}, \dot{q}, \lambda, u, q, t; \overline{u}, \overline{q}) = 0 \tag{7}$$

and satisfies the following two conditions to capture the perturbation direction with minimum resistance

$$\frac{\partial \boldsymbol{F}}{\partial \overline{u}} = 0 \quad \frac{\partial \boldsymbol{F}}{\partial \overline{q}} = 0 \tag{8}$$

We use the following two expressions to be recorded as

$$\gamma_u = [-\boldsymbol{Q}]_u$$

$$\gamma_q = [\boldsymbol{M}\dot{u} + \boldsymbol{P}\lambda - \boldsymbol{Q}]_q$$

and get then the following system equations

$$\begin{bmatrix} \boldsymbol{M} & 0 & \boldsymbol{P} & \gamma_u & \gamma_q \\ 0 & \boldsymbol{T} & 0 & -\boldsymbol{I} & [\boldsymbol{T}\dot{q}]_q \\ \ddot{\boldsymbol{C}}_{\dot{u}} & 0 & 0 & \ddot{\boldsymbol{C}}_u & \ddot{\boldsymbol{C}}_q \\ 0 & 0 & 0 & \dot{\boldsymbol{C}}_u & \dot{\boldsymbol{C}}_q \\ 0 & 0 & 0 & 0 & \boldsymbol{C}_q \\ 0 & 0 & 0 & \boldsymbol{B}_1 & 0 \\ 0 & 0 & 0 & 0 & \boldsymbol{B}_0 \end{bmatrix} \begin{bmatrix} \dot{u}_{\overline{u}} & \dot{u}_{\overline{q}} \\ \dot{q}_{\overline{u}} & \dot{q}_{\overline{q}} \\ \lambda_{\overline{u}} & \lambda_{\overline{q}} \\ u_{\overline{u}} & u_{\overline{q}} \\ q_{\overline{u}} & q_{\overline{q}} \end{bmatrix} = \begin{bmatrix} 0 & 0 \\ 0 & 0 \\ 0 & 0 \\ \boldsymbol{I} & 0 \\ 0 & \boldsymbol{I} \end{bmatrix} \tag{9}$$

The requirements of proper MBS modeling are thus put forward. Specifically, the more accurate modeling of complex constraints is constantly carried out by applying the graph of topological relationship, and the more precise analyses of associated inner forces are calculated by using the improved variable-step integral algorithm. Therefore, the dynamic design methodology is a series of systematic methods that are based on the accurate analysis results of complex constraint inner forces.

Negrut's contribution is to better understand the reduction transactions based on POD (Proper Orthogonal Decomposition), which can only be implemented under the specified steady state without singularities of complex constraints. However, since the (near-) linear and nonlinear relationship of wheel-rail contact is dialectical, the application of PODA should first remove and eliminate the mutual influences of nonlinear vibrations by conducting the optimal parameter configuration of higher speed bogies. Only in this way can the self-adaptive improved design of higher speed bogies scientifically promote the limit and construction speeds under the rational condition of wheel-rail matching, which is one of the roles of the following visual data mining tool.

Every quasi-static state with constant speed at the specific λ_e is assumed to be the following equations for the rail vehicle MBS system shown in Equation (10)

$$\boldsymbol{F}(q, \dot{q}, t) = 0 \tag{10}$$

where $y, \dot{y}$ represents all state variables and associated derivatives.

At the working point, $q = q^k$ and $\dot{q} = \dot{q}^k$, the first order difference formula of Equation (10) is given as follows

$$\left[\left. \frac{\partial \boldsymbol{F}}{\partial q} \right|_{q^k, \dot{q}^k} + \frac{1}{h\beta_0} \left. \frac{\partial \boldsymbol{F}}{\partial \dot{q}} \right|_{q^k, \dot{q}^k} \right] \Delta q = -\boldsymbol{F}(q, \dot{q}, t) \tag{11}$$

where β_0 is the scalar constant, that is related to the integrator order; Δq is the corrected difference direction; h is the integration step size; $-\boldsymbol{F}$ is the residual part of Equation (10), which represents the imbalance degree of the force system.

The left matrix of Equation (11) is the Jacobean matrix on the required quasi-equilibrium state, i.e., the Jacobean matrix of first-index DAEs for Equation (1)

$$\boldsymbol{\Gamma} = \begin{bmatrix} \frac{\boldsymbol{M}}{h\beta_0} - \boldsymbol{C}_u & \boldsymbol{M}_q\dot{u} + \boldsymbol{C}_{qq}^T\lambda - \boldsymbol{Q}_q & \boldsymbol{C}_q^T \\ \boldsymbol{I} & -\frac{1}{h\beta_0} & \boldsymbol{0} \\ \boldsymbol{0} & \boldsymbol{C}_q & \boldsymbol{0} \end{bmatrix} \tag{12}$$

where $\boldsymbol{I}$ is the unit matrix; u, q, qq are subscripts, i.e., the first or second-order partial derivatives of (non-) holonomic constraints $\boldsymbol{C}$ to u/q.

Accordingly, the MBS eigenvalue solution $Eig(\boldsymbol{\Gamma})$ can be obtained by orthogonal decomposition. Some analysis software can provide systemic modal analysis tools, i.e., root-locus graphs of closed-loop nonlinear systems. The disciplinary surrogate models used

herein to approach the (near-) linear relationship of wheel-rail contact, i.e., the geometric linearity between wheel-rail contact, are represented by mono-curvature contact between wheel and rail arcs.

The HSR practices must grasp the dialectical relationship between (near-) linearity and nonlinearity of wheel-rail contact. The (near-) linear surrogate model of wheel-rail contact is composed of such parameters as λ_e, which is the equivalent parameter given by the RRD (Rolling Radius Difference) curve of the wheelset, similar to the AC voltage of 220/380 V. The nominal equivalent conicity λ_{eN} refers to the equivalent conicity with a wheelset hunting displacement amplitude of 3 mm under the specific wheel-rail profile matching. For rail 60E1/wheel S1002, with the back-to-back distance of 1360 mm and bottom inclination of 1/20, $\lambda_{eN} \approx 0.01$ and the track window becomes narrower. While considering rail CN60KG/wheel XP55 with the back-to-back distance of 1353 mm and bottom inclination of 1/40, $\lambda_{eN} \approx 0.06$ and track window becomes wider.

For the worn wheels and rails, the actual equivalent conicity λe will be affected by two aspects due to the variation of the RRD curve: firstly, when the negative slope at the zero crossing point causes the local conformal contact at one side of rail gauge corner, which in turn transforms into frictional heat loss and eventually evolves into the local RCF (Rolling Contact Fatigue) failure or plastic flow; secondly, when the discontinuity at the zero crossing point occurs, the local conformal contact is constituted on the top of the railhead, which will occasionally force the wheelset to form the small-amplitude hunting oscillation and gradually constitute the sufficiently strong external excitation source.

Compared with the conventional root locus graph, the analysis graph of full-vehicle stability properties and variation patterns has three important features: i.e., closed-loop pole, stability margin (or critical damping), and convected motion relationship. The convected motion relationship refers to the convected motion formed between relevant modes caused by the complex constraint singularity in the generalized space, which constitutes the corresponding kinetic energy exchange or transformation.

Generally, the nonlinear systems no longer meet the following requirements, i.e., modal orthogonality and mode shape symmetry or anti-symmetry. The convected motion relationship depends on the ill-conditioned number of the Jacobian matrix. Instead of the genetic algorithm or particle swarm algorithm, the analysis graph of full-vehicle stability properties and variation patterns is the best tool for optimal parameter configuration of higher speed bogies because the PODA technique effectively solved the difficult acquisition problem of snapshot matrices in the POD transacting processes. Specifically, the PODA technique is applied in the optimal parameter configuration of higher speed bogies so as to eliminate the adverse convected motion relationship and make the beneficial one more robust.

2.2. Inherent Rigid-Flex Coupling Relation of HSRS

The improved transaction strategy of the flexible body to MBS interface by using MMAT has enriched the intension of the surrogate model. Specifically, by applying the CMS (Component Mode Synthesis) method, both interface displacement condensation treatment and CC (Characteristic Constraint) mode make the surrogate model of a flexible body neater to deal with the nonlinear influence factors on relevant interfaces [31,32], so as to implement the robust design of lightweight structures [33].

As shown in Equations (4) and (5), the hypothesis of classic structural dynamics is changed from the linear elastic deformation under the service condition of small displacement to the one under the large displacement service system, and the modal analysis of the rigid-flex coupling system includes two subsets of motion and elasticity. Under the changed assumption of linear elastic deformation under large displacement service systems, large-scale nonlinear systems will have the inherent rigid-flex coupling relationship due to the singularities or complex constraints.

For a linear elastic system with total n DoFs (Degree of freedom), Q is taken as the interface DoFs, and P is the internal DoFs, $n = Q + P$, which are represented by subscripts o

and i, respectively. The displacement $x_o = X_o e^{j\omega t}$ on the interface DoFs, the displacement $x_i = X_i e^{j\omega t}$ on the internal DoFs, and the excitation load $f_o = F_o e^{j\omega t}$ acting on the interface DoFs. Without considering damping for the time being, the motion equation of the service system of a lightweight structure can be written in the following block form [34]:

$$\begin{bmatrix} M_{ii} & M_{io} \\ M_{oi} & M_{oo} \end{bmatrix} \begin{Bmatrix} \ddot{x}_i \\ \ddot{x}_o \end{Bmatrix} + \begin{bmatrix} K_{ii} & K_{io} \\ K_{oi} & K_{oo} \end{bmatrix} \begin{Bmatrix} x_i \\ x_o \end{Bmatrix} = \begin{Bmatrix} 0_P \\ f_o \end{Bmatrix} \tag{13}$$

where $\boldsymbol{M}$, $\boldsymbol{K}$, $\ddot{\boldsymbol{x}}$ and $\boldsymbol{x}$ are the mass matrix, stiffness matrix, acceleration and displacement response of service system respectively, 0 is the zero vector matrix, and the subscripts represent the number of rows and columns.

The displacement $\boldsymbol{x}$ of service system can be extended to the linear combination of inherent modes and constrained modes for the fixed interface with mass normalization.

Inherent modes $\boldsymbol{\Phi} = [\Phi_1 \quad \cdots \quad \Phi_P]$.

Constrained modes $\begin{bmatrix} \boldsymbol{\Psi} & \boldsymbol{I}_{Q\times Q} \end{bmatrix}^T$ and $\boldsymbol{\Psi} = -K_{ii}^{-1} K_{io} = \begin{bmatrix} \Psi_1 & \cdots & \Psi_Q \end{bmatrix}$.

The relationship between generalized displacement $\begin{Bmatrix} \eta_i & x_o \end{Bmatrix}^T$ and physical displacement $\begin{Bmatrix} x_i & x_o \end{Bmatrix}^T$ is as follows:

$$\begin{Bmatrix} x_i \\ x_o \end{Bmatrix} = \begin{bmatrix} \boldsymbol{\Phi} & \boldsymbol{\Psi} \\ \boldsymbol{0}_{Q\times P} & \boldsymbol{I}_{Q\times Q} \end{bmatrix} \begin{Bmatrix} \eta_i \\ x_o \end{Bmatrix} = \boldsymbol{T} \begin{Bmatrix} \eta_i \\ x_o \end{Bmatrix} \tag{14}$$

Substitute Equation (14) into Equation (13), left multiple by $\boldsymbol{T}^T$, and transform the system motion equation into a description form based on generalized displacement

$$\begin{bmatrix} \overline{M}_{ii} & \overline{M}_{io} \\ \overline{M}_{oi} & \overline{M}_{oo} \end{bmatrix} \begin{Bmatrix} \ddot{\eta}_i \\ \ddot{x}_o \end{Bmatrix} + \begin{bmatrix} \overline{K}_{ii} & \overline{K}_{io} \\ \overline{K}_{oi} & \overline{K}_{oo} \end{bmatrix} \begin{Bmatrix} \eta_i \\ x_o \end{Bmatrix} = \begin{Bmatrix} 0_P \\ \overline{f}_o \end{Bmatrix} \tag{15}$$

where

$$\begin{gathered} \overline{M}_{ii} = \boldsymbol{\Phi}^T M_{ii} \boldsymbol{\Phi} = \boldsymbol{I}_{P\times P} \\ \overline{M}_{io} = \overline{M}_{oi}^T = \boldsymbol{\Phi}^T M_{ii} \boldsymbol{\Psi} + \boldsymbol{\Phi}^T M_{io} \\ \overline{M}_{oo} = \boldsymbol{\Psi}^T M_{ii} \boldsymbol{\Psi} + \boldsymbol{\Psi}^T M_{io} + M_{oi} \boldsymbol{\Psi} + M_{oo} \\ \overline{K}_{ii} = \boldsymbol{\Phi}^T K_{ii} \boldsymbol{\Phi} = \Lambda_{ii} \\ \overline{K}_{io} = K_{oi}^T = \boldsymbol{\Phi}^T K_{ii} \boldsymbol{\Psi} + \boldsymbol{\Phi}^T K_{io} = \boldsymbol{0}_{P\times Q} \\ \overline{K}_{oo} = \boldsymbol{\Psi}^T K_{ii} \boldsymbol{\Psi} + \boldsymbol{\Psi}^T K_{io} + K_{oi} \boldsymbol{\Psi} + K_{oo} = K_{ii} \boldsymbol{\Psi} + K_{oo} \\ \overline{f}_o = f_o \end{gathered}$$

Suppose that $\Lambda_{ii} = diag(\omega_1^2, \quad \cdots \quad \omega_k^2, \quad \cdots \quad \omega_P^2)$, ω_k^2 is the k-th inherent vibration frequency of service system under the condition that all DoFs on the interface are constrained.

Introducing the modal damping ratio ζ_k, $k = 1, 2, \cdots P$, the first line of Equation (15) can be expanded into P independent equations

$$\ddot{\eta}_k + 2\zeta_k \omega_k \dot{\eta} + \omega_k^2 \eta_k = -L_k \ddot{\delta}_k \tag{16}$$

where the modal participation factor under multi-axial excitation

$$L_k = \boldsymbol{\Phi}_k^T M_{ii} \boldsymbol{\Psi} + \boldsymbol{\Phi}_k^T M_{io} \tag{17}$$

Substituting $\eta_k = \Pi_k e^{j\omega t}$ and $\ddot{\delta}_k = -\omega^2 \Delta_k e^{j\omega t}$ into Equation (16), the result can be obtained after sorting

$$\Pi_k = \frac{1}{\left(\frac{\omega_k}{\omega}\right)^2 + 2j\zeta_k \frac{\omega_k}{\omega} - 1} L_k \Delta_k = H_k L_k \Delta_k \tag{18}$$

According to Equation (18), perform the MSR correctly based on node force and displacement in global coordinates and draw von Misses dynamic stress cloud. Through effective modal excitation $\ddot{\delta}_k$, the seamless integration with Dong's structure stress recovery and collaborative operation with weldline fatigue assessment are realized under the technical support of relevant analysis softwares [35,36].

The relationship between loading excitation and displacement/acceleration response of the interface can be obtained from the second line of Equation (15):

$$\overline{\boldsymbol{K}}_{oo}\boldsymbol{X}_o + \left(\sum_{k=1}^{P} H_k L_k^T L_k\right)\ddot{\boldsymbol{X}} + \overline{\boldsymbol{M}}_{oo}\ddot{\boldsymbol{X}}_o = \boldsymbol{F}_o \tag{19}$$

in which, the stiffness matrix of the interface after reduction is weakened by the definition of interface DoFs, i.e.,

$$\overline{\boldsymbol{K}}_{oo} = \boldsymbol{K}_{oo} - \boldsymbol{K}_{io} \tag{20}$$

where $\boldsymbol{M}_{oo}$ is Guyan mass matrix, in a specific response surface direction l_r, the mass or moment of inertia of rigid body $\boldsymbol{m}_T = l_r^T \boldsymbol{M}_{oo} l_r$, and the mass matrix of the interface after reduction is enhanced by the definition of interface DoFs,

$$l_r^T \overline{\boldsymbol{M}}_{oo} l_r > l_r^T \boldsymbol{M}_{oo} l_r \tag{21}$$

If the weak coupling interfaces of the service system have only one node (no constrained DoF), the constrained mode is composed of six rigid body motion modes, and Equation (19) can be converted into the loading excitation and acceleration response of the interface as follows

$$\left(\sum_{k=1}^{P} H_k L_k^T L_k + \overline{\boldsymbol{M}}_{oo}\right)\ddot{\boldsymbol{X}}_o = \left(\sum_{k=1}^{P} H_k M_k^{eff} + \overline{\boldsymbol{M}}_{oo}\right)\ddot{\boldsymbol{X}}_o = F_{o\min} \tag{22}$$

where $L_k^T L_k$ is the effective mass of the k-th inherent mode of service system, it can be noted as M_k^{eff}; and $F_{o\min}$ is referred as the minimum amplitude of excitation load acting on the interface DoFs.

In terms of dynamic response design optimization of lightweight structures, the above deduction of inherent rigid-flexible coupling relationship has the following three important significances: (i) The weak coupling interface to the service system is one of the important prerequisites for determining the ESL sets; (ii) The boundary loading treatment is one of the effective methods for FEM updating; (iii) The MMRT efficient tool can ensure the MSR correctness under the inherent rigid-flex coupling relationship.

According to the inherent rigid-flex coupling relationship of HSRS, as shown in Equations (19) and (22), the methods of modal superposition and virtual excitation have lost their associated application premises and are no longer applicable to fatigue load assessments. However, for instances of steel structures used in tall buildings, platforms for offshore drilling, and road vehicles, the linear elastic deformation hypothesis is held under the small displacement service system, so the above two fatigue load assessment methods are still applicable [37,38].

2.3. Flow Chart of Large-Scale MDO Such as HSRS

The flow chart of large-scale MDOs such as HSRS using dynamic design methodology is shown in Figure 2, which includes three contributions to collaborative innovations among different disciplines.

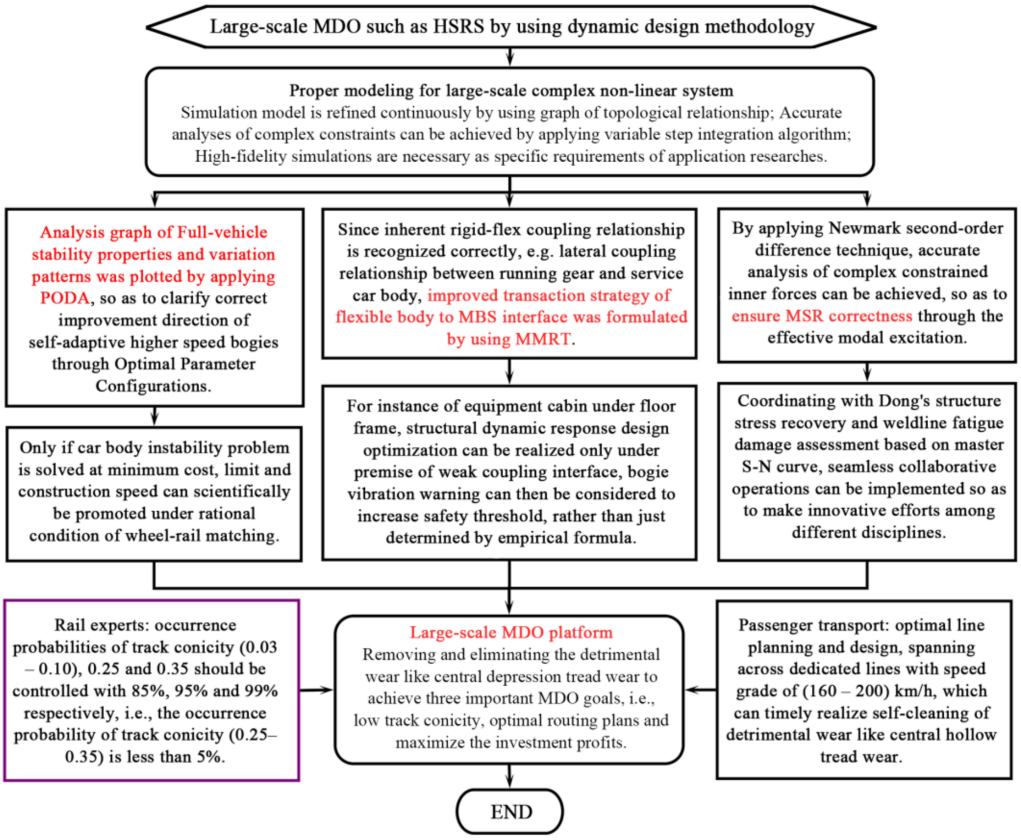

Figure 2. Flow chart of large-scale MDO such as HSRS by using dynamic design methodology.

In summary, detrimental wear is one of the technical bottlenecks in worldwide HSR practices. However, as for Chinese high-tech manufacturing industries such as HSRS, our own particularities must be paid much attention to, e.g., central hollow tread wear. For this reason, the dynamic design methodology should be actively recommended and introduced in Chinese HSR practices so as to achieve the three important MDO goals of large-scale complex nonlinear dynamic systems. Especially for present engineering experiences and techniques or various kinds of analysis software, it is necessary to take care of their adaptation conditions or application prerequisites.

3. Correct Direction of Chinese HSRS Improved Design

3.1. Rational Condition of Wheel-Rail Matching

In view of the particularities of Chinese HSR practices, i.e., the back-to-back distance of wheelset, L = 1353 mm, and the improper ratio of curve to tangent in route planning on dedicated lines, the rational condition of wheel-rail matching should be as follows: the nominal equivalent conicity $0.10 \geq \lambda_{eN} > \lambda_{emin}$, and the minimum allowable equivalent conicity λ_{emin} = (0.03–0.06). This rational condition can be determined by referring to relevant experiences at home and abroad.

Although bogie articulated and car body tilted are two key technologies for speeding up on the present European rails, the rail grinding treatment is one of the important preconditions for their implementation. For the practices of Japanese Shinkansen or speeding up on the present European rails, although the bottom inclinations are different, but L = 1360 mm in general. When the wheel standard profile S1002 is matched to UIC rail 60E1 with a bottom inclination of 1/20, λ_{eN} = 0.01. However, as shown in Figure 3a,b,d, the tight track gauge or narrow track window is formed between them, the negative influences of which are eliminated by rail grinding or wheel renewal profiles.

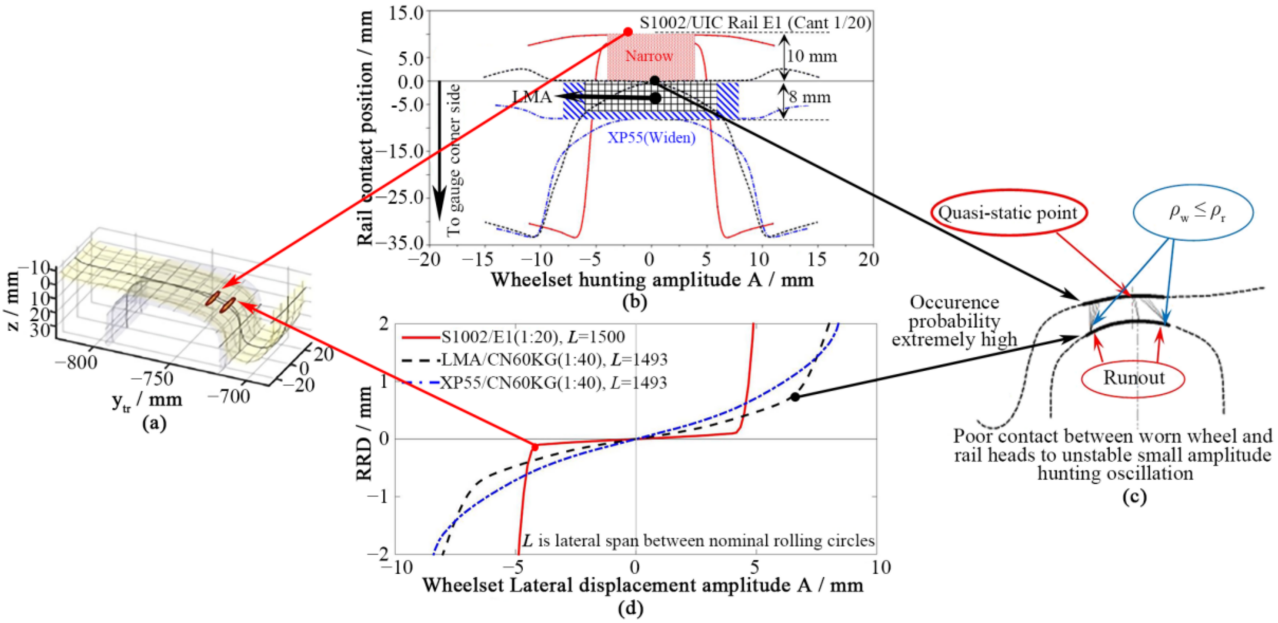

Figure 3. Influences of track parameters on low wear area of wheel-rail contact and detrimental wear evolution. (**a**) Two-point contact problem on rail shoulder at one side of gauge corner such as flange root and side wear. (**b**) Comparison of three typical wheel-rail matching situations for contact point variation on railhead. (**c**) Two-point contact problem on railhead top with stronger dynamic interaction such as central hollow tread wear in Chinese HSR practices. (**d**) Comparison of RRD curves for three typical wheel-rail matching situations.

Relatively speaking, the operation and maintenance practices of French TGV/AGV trains have a more appropriate technical economy, and the survey of service lines shows two areas with a relative higher probability distribution density of low and high track conicity [39]. These are closely related to the techniques of articulated bogies and longitudinal damping between inter-vehicles. The articulated bogies have a 3 m wheelbase and are configured with 2 anti-yaw dampers per bogie to ensure the stability performance of bogies at higher equivalent conicity. Meanwhile, there are four longitudinal dampers installed in the upper and bottom parts between inter-vehicles to remove and eliminate the car body instability at lower equivalent conicity.

For the dedicated lines with a speed grade $\geq$ 230 km/h [39], there are two extreme cases as follows:

(1) Italian ETR600 train requires that the track conicity after rail grinding be less than 0.05, tries to achieve the expected goal of uniform wear stage at an extraordinary cost, and the maximum speed can reach 300 km/h in mountain lines. After the acquisition of tilting techniques from FIAT, the first ETR 600 tilting train launched by ALSTOM switched to traditional anti-yaw dampers, i.e., the mechanism of large damping to suppress hunting. However, an active control technique of lateral and roll integrated suspension may be developed when considering the car body instability that occurred occasionally at low conicity [40].

(2) German ICE3 train requires that the occurrence probability of track conicity 0.10, 0.20, and 0.30 is 50%, 95%, and 99%, respectively. However, the rail grinding treatment unexpectedly acquires the stable wear stage at a high conicity of λ_e = (0.25–0.35), and the period of wheelset re-profiling under the floor is extended to (35–45) $\times$ 10^4 km [39].

The general regulations presented in the wear survey of worldwide wheel-rail contact are as follows: wheel hollow tread and railhead top crown, i.e., curvature radius is varied from 350 mm to 150 mm [41]. The radical reason for implementing one kind of wheel-rail matching or the other is often institutional inertia—a strong tendency to continue doing what has been completed in the past. But the impacts of wheel and rail profiles on the

performance of the vehicle/track interaction are large and the decision should not be made lightly.

For instance, the profile evolution from P8 to P12 tread in UK HSR practices fully demonstrates the importance of scientifically promoting the limit and construction speeds under the rational condition of wheel-rail matching [42–45]. Similar to the practices of Japanese Shinkansen rails, UK HSR has not undergone rail grinding treatment, i.e., UIC60E1 with a bottom inclination of 1/20. In order to reduce the RCF failure on rail shoulder at one side of gauge corner, the P8 tread is selected for wheels, by which the stable wear regulation at high conicity is represented in the operation and maintenance of such as the Mark 3 train and EMU trainset [39].

First of all, the Express Rails to London Heathrow Airport borrowed partially from the rapid rail system. The light rails UIC56E1 with a bottom inclination of 1/20 will be matched to the P8 tread, the flange thickness of which is reduced from the original 32 mm to 28 mm, and the flange angle is reduced from the original 76 deg to 68 deg. As a result, the wheel-rail clearance on each side is increased by 4 mm, and $\lambda_{eN} \approx 0.18$.

Secondly, the P8 adopts a specific hollow tread with a larger curvature radius. However, it is still easy to form the local conformal contact (or two-point contact) on the rail shoulder at one side of the gauge corner. Particularly, the railhead damage is difficult to avoid when the curving negotiation has a small radius. As such, the wheel spin singularity forces the tread to gradually generate the uneven power dissipation problem, i.e., the RCF fails on the flange root or rail shoulder, which is the unbearable cost that must be paid during the stable wear stage at high conicity.

Finally, the proposal was adopted to replace the P8 tread with the P12 one, so as to implement the economical re-profiling of the wheelset, which has the following four features: (i) The anti-RCF design near to flange root is used to avoid the two-point contact on rail shoulder as much as possible; (ii) The flange thickness is further reduced by 2 mm, which matches to the UIC 56E1 with bottom inclination of 1/20, and $\lambda_{eN} \approx 0.10$; (iii) Moreover, UIC60E2 with bottom inclination of 1/40 is partially changed in UK HSR to form hammering impacts, but the rail gauge is broadened to 1438 mm, to which the P12 tread with flange thickness of 26 mm is matched, $\lambda_e < 0.10$; (iv) So the economic re-profiling option of wheelset is implemented with the assistance of auxiliary technologies such as proper flange grease spraying [46], and the wheelset re-profiling period is extended twice.

Chinese HSR practices should not blindly copy these foreign experiences because the Chinese track parameter system has already achieved the technical objective of their improved designs for wheel-rail relationships. No matter the car body instability or the bogie yaw phase margin deficiency, the improper application of anti-roll torsion bar devices has become one of the most common technical problems in Chinese HSR practice, which may be caused by the long-term operation of dedicated lines.

Both practices of CRH in China and KTX in South Korea can confirm that the XP55 tread is one of the optimal wheel profile designs to better fit the wheelset change, i.e., L = 1353 mm. If the XP55 tread is matched to the rail CN60KG with a bottom inclination of 1/40, as shown in Figure 3b–d, $\lambda_{eN} \approx 0.06$, and the corresponding low wear area is also significantly expanded. Under operations at servicing speeds $\leq$200 km/h, the wheelset re-profiling period can generally reach 30×10^4 km.

However, CRH5 (including anti-wind/sand trainset) has experienced car body shaking when the servicing speed is increased to 250 km/h on some dedicated lines. Considering the constant speed hypothesis, the falling-off accident of a long transmission shaft may occur again. Specifically, λ_e may be decreased after rail grinding, which causes the service car body to roll and rock. So, the negative influences will be produced feedback to the creepage and wear of corresponding wheels through anti-roll dual-bar per bogie. Meanwhile, the improper ratio of curve to tangent forces the wheels to rapidly form the central hollow tread wear when considering two traction motors suspended under floor frame (the maximum weight is ca. 58 t for the service car body). Under the influence of wheel spin singularity,

small-amplitude hunting oscillation causes the bogie frame to produce lateral forced vibration with a dominant frequency of ca. 7.0 Hz.

Similarly, the CRH1 model manufactured by BST (Bombardier Sifang (Qingdao) Transportation Ltd., Qingdao, China) has been cancelled. After two inclined-mounted dampers in the prototype design were removed between inter-vehicles, λ_{eN} was wrongly raised from 0.03 to 0.12, resulting in the bogie vibration alarm.

3.2. Primary Hunting Phenomenon in German ICE3 Serial Bogies

The analysis graph of full-vehicle stability and variation patterns should guide instructively the optimal parameter configuration of higher speed bogies, as shown in Figure 4, formulating the major issue to be clarified in developing large-scale complex nonlinear dynamic systems such as the ICE3 serial bogie and furthermore making strategic decisions on self-adaptive improved design.

As for the prototype design of German ICE3 serial bogies, as shown in Figure 4a, we cannot overlook the following three main technical features: (i) The strong rigid constraint of wheelset positioning is constructed by a rotary arm axlebox, i.e., longitudinal/lateral stiffness is 120/12.5 MN/m per axlebox; (ii) Anti-hunting redundancy design of four novel anti-yaw dampers per bogie is adopted, such as ZF Sachs T60/T70 with dual-/mono-circulation, producing differently the anti-hunting high-frequency independence interactions; (iii) Two traction motors per bogie are assembled with hanging frame, through the lateral swing of which the generalized mass participated in the instability hunting oscillation of motor bogies can be reduced remarkably.

As shown in Figure 2b,c, literature [47] confirms that the technical prototype of German ICE3 serial bogies has the primary hunting design default, which has three important meanings as follows:

(1) The vehicle and rail experts have quite a difference of opinions. As shown in Figure 2d,e, the irrational condition of wheel-rail matching should be improved by rail grinding with railhead profile modification, e.g., symmetrical trimming of railhead 60 N [48]. Considering our own particularities, the rail grinding treatment makes it impossible to remove or eliminate the central hollow tread wear and associated negative impacts.

(2) However, when the thick flange S1002G tread (or S1002CN, flange thickening by 3.5 mm) is replaced with a thin flange re-profiling one and λ_{eN} = 0.17, as shown in Figure 2f–g, the central hollow tread wear is constructed gradually in the long-term operations on the dedicated lines of high-speed grade. In particular, the wheel tread of the bogies under ZF SachsT70 configuration for long-formation train forms the central hollow tread wear with dual light bands.

(3) Different from the tight track gauge or narrow track window such as the German ICE rail system, Chinese HSR practices need to undergo the intensive research on the wheel-rail relationship, i.e., singularities of anti-roll complex constraints and associated negative influences that feedback to the creepage and wear of corresponding wheels. Especially for mountain lines, open and dark lines are staggered, and unsteady aerodynamic loads will force the primary hunting phenomenon to turn into the secondary hunting phenomenon, which will lead to high-speed car body shaking at low conicity.

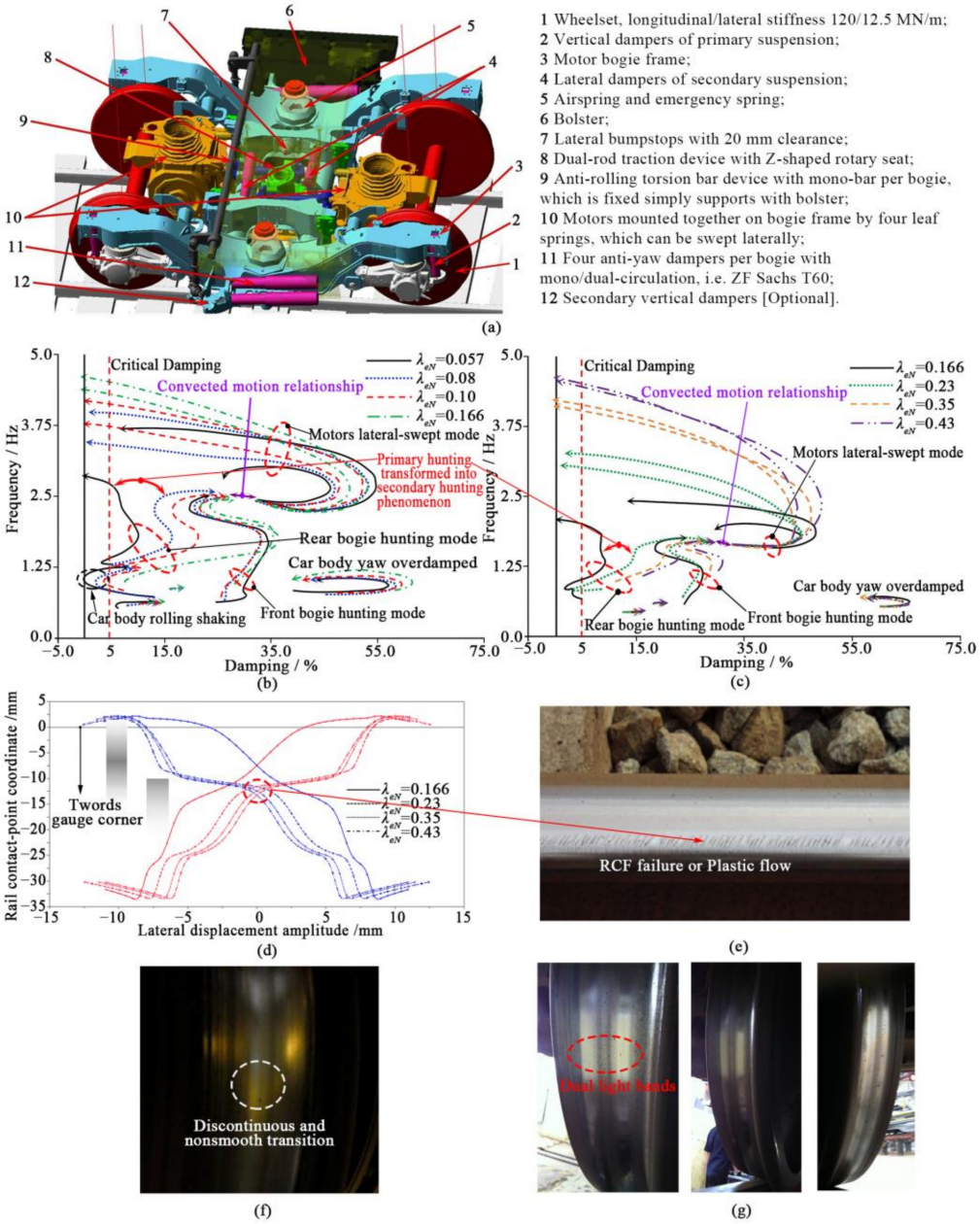

Figure 4. Primary hunting design default of German ICE3 series bogies prototype and associated negative influences feedback to creepage and wear of corresponding wheels. (**a**) Template model of ICE3 motor bogies and associated components. (**b**) Analysis graph of motor vehicle stability properties and variation patterns under the following configuration, i.e., Four ZF Sachs T60 anti-yaw dampers per bogie and radial stiffness of 70 MN/m for both end rubber joints. (**c**) Analysis graph of motor vehicle stability properties and variation patterns under the following configuration, i.e., Four ZF Sachs T70 anti-yaw dampers per bogie and radial stiffness of 25 MN/m for both end rubber joints. (**d**) Irrational condition of wheel-rail matching. (**e**) RCF failure or plastic flow on rail shoulder at one side of gauge corner. (**f**) Central hollow tread wear under ZF Sachs T60 configuration. (**g**) Hollow tread wear with dual light band under ZF Sachs T70 configuration. Both tread wear characteristics (**f**,**g**) are related to thin flange re-profiling.

For the anti-roll torsion bar devices adopted in German ICE3 serial bogies, as shown in Figure 5a,b, the torsion bar is placed on top, by which the fixed or floating simple support can be constructed on the bolster.

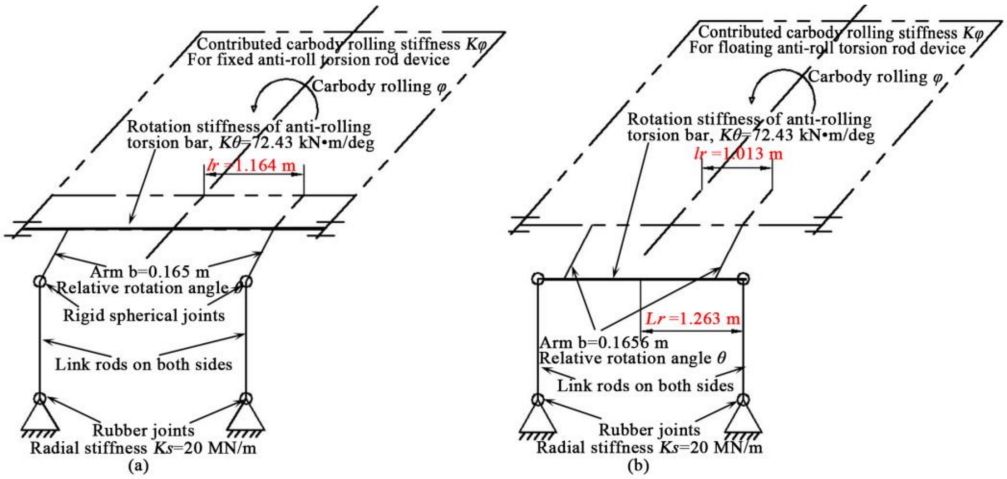

Figure 5. Diagram of anti-roll torsion bar device: (**a**) Anti-roll torsion bar device with fixed simply supported on bolster; (**b**) Anti-roll torsion bar device with floating simply supported on bolster.

The torsion bar itself does not work when running in tangent lines or in large radius curving negotiation. While running through transition curves, turnouts, or trains passing each other, the roll and rock of service car body occur, resulting in the torsion bar being twisted and deformed. As such, the stiffness contribution of the fixed, simply supported torsion bar is ca. (1.4–1.5) times that of the floating, simply supported one, which becomes the selection for ICE3 serial bogies.

The lower rubber joints of the link rods on both sides have a radial stiffness of ca. 20 MN/m, the stiffness contribution of which is ca. 1.0 MN·m/deg to the service car body roll. Compared with the modal parameters calculated by dynamic simulation analyses, the relative error of these computed results is only (5.0–6.0)%, details seen in Table 1.

Table 1. Anti-roll torsion bar devices to car body roll stiffness contributions with Fixed/floating simply supported on bolster of bogie.

Different Installation of Anti-Roll Torsion Bar Simply Supported on Bolster of Bogie	Bar-System Calculation, Torsion Stiffness K_θ = 72.43 kN·m/deg			Equivalent Stiffness Obtained from Dynamical Simulation Analyses When Running on Tangent Lines or Negotiating through Large Radius Curves	Relative Error %
	Radial Stiffness of Rubber Joints at Lower End of Link Rods on Both Sides, K_s = 20 MN/m	Radial Stiffness of Rubber Joints at Lower End of Link Rods on Both Sides, $K_s \to \infty$	Equivalent Stiffness When Running on Tangent Lines or Negotiating through Large Radius Curves		
Fixed	0.935	14.3	0.87	0.92	6.0
Floating	1.11	10.8	1.01	1.06	4.7

Note: the rubber joints or anti-roll torsion bar to car body rolling stiffness contribution is calculated respectively and the equivalent stiffness is then given in serial connection, unit in MN·m/deg.

Special attention: the UK small defect spectrum is used as the track irregularity excitation input for the dedicated lines of speed $v > 200$ km/h. For the dedicated line of 160 km/h $\leq v < 200$ km/h, the German track spectrum of high interference is used as the track irregularity excitation input. And in the speed range of (80–140) km/h, the fifth-grade American track spectrum (AAR5) is used as the track irregularity excitation input. These descriptions do not repeat themselves in other simulations in this paper.

To sum up, due to the primary hunting design default existed in the prototype of ICE3 serial bogies, the practices of German ICE rails have achieved the unexpected gains of stable wear stage at high conicity by using rail grinding treatment under the rail system of tight track gauge or narrow track window. Nevertheless, considering our own particularities, the rail grinding treatment brings the following three negative results to Chinese HSR practices: (i) After the rail grinding treatment of the Beijing-Shanghai HSR dedicated line, all of the bogie wheels for long-formation trains change to the flange side wear, and the RCF failure or plastic flow occurs on the rail shoulder at one side of gauge corner when run-

ning in tangent line or in large-radius curving negotiations; (ii) When λ_e < (0.10–0.12), the high-speed shaking phenomenon will occur at low conicity, resulting in serious vibration comfort problems, so we have to abandon this high-quality resource of wheel-rail matching; (iii) Although the wheels are changed to adopt the renewal profile design LMB-10, when λ_e is approaching to (0.30–0.35), the central hollow tread wear inevitably forms the characteristics of almost no flange root wear or flange side wear, occasionally resulting in the more and more serious fluttering phenomenon.

3.3. Fluttering Formation Mechanism of Service Car Body System

Due to the central hollow tread wear, the worn wheel-rail occasionally constructs the local conformal or bad contact on some sections, and the small amplitude hunting oscillations of wheelsets make the CRH3C bogie frame produce the lateral forced vibration response with the dominant frequency of ca, (7.0–8.0) Hz and the leading frequency of more than 10 Hz. Therefore, unlike the practices of German ICE rails, the central hollow tread wear is the detrimental wear unique to Chinese HSR practices, by which a sufficiently strong external excitation source is occasionally formed.

Under these lateral excitations from running gear, the lateral movement of the service car body becomes the perturbation direction with minimum resistance, as shown in Figures 6 and 7, and causes the lateral coupling resonance of the traction converter in the equipment cabin under the floor frame, ca. (9.2–9.3) Hz. As a result, the self-weight wedge tight failed on some rubber hanging joints, and the reciprocating lateral movements of the traction converter released the corresponding kinetic energy in time, which did not have any substantial impact on the aluminum alloy car body. Unlike the situation on German ICE rails, the improvements of the corresponding imported technique should take into account the particularities of Chinese HSR practices, increasing moderately in the lateral modal frequency of the traction converter hanged under the floor frame.

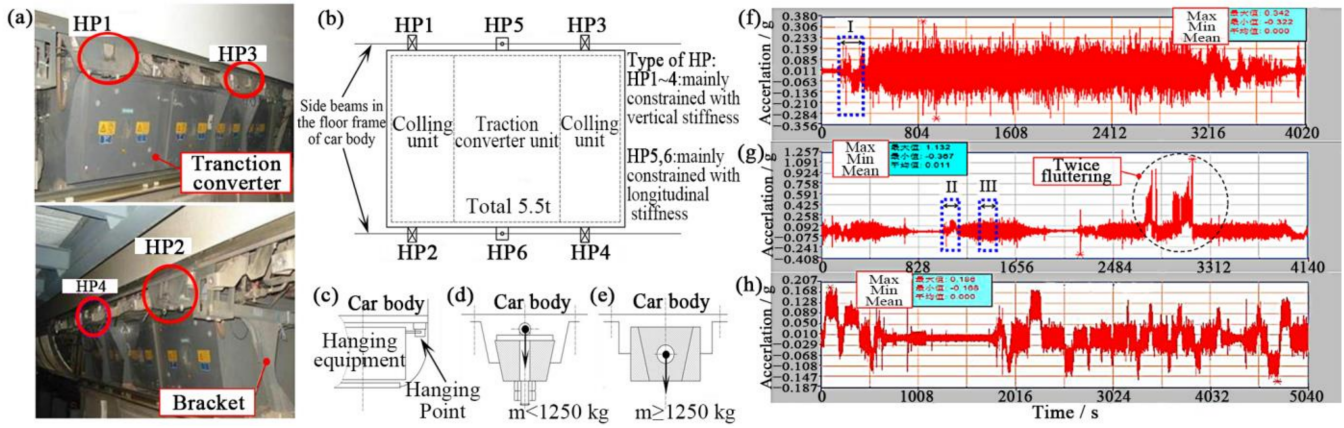

Figure 6. Tracking test and measuring results of first fluttering phenomenon produced in service car body when running from Dalian to Harbin. (**a**) Acceleration measured at hanging points of HP (1–4). (**b**) HP arrangement of traction converter with dual cooling units (ca.6.6 t). (**c**) Equipments hanged with side beams in floor frame; (**d**) Conic rubber hanger with bolt pre-tightening for $m \leq 1250$ kg. (**e**) Wedge rubber hangers with pre-tightening by self-weight for m>1250 kg. (**f**) Stationary acceleration time history of traction converter hanged under floor frame. (**g**) Critical acceleration time history with two fluttering phenomena; (**h**) Nonstationary time history with lateral reciprocating motions of traction converter.

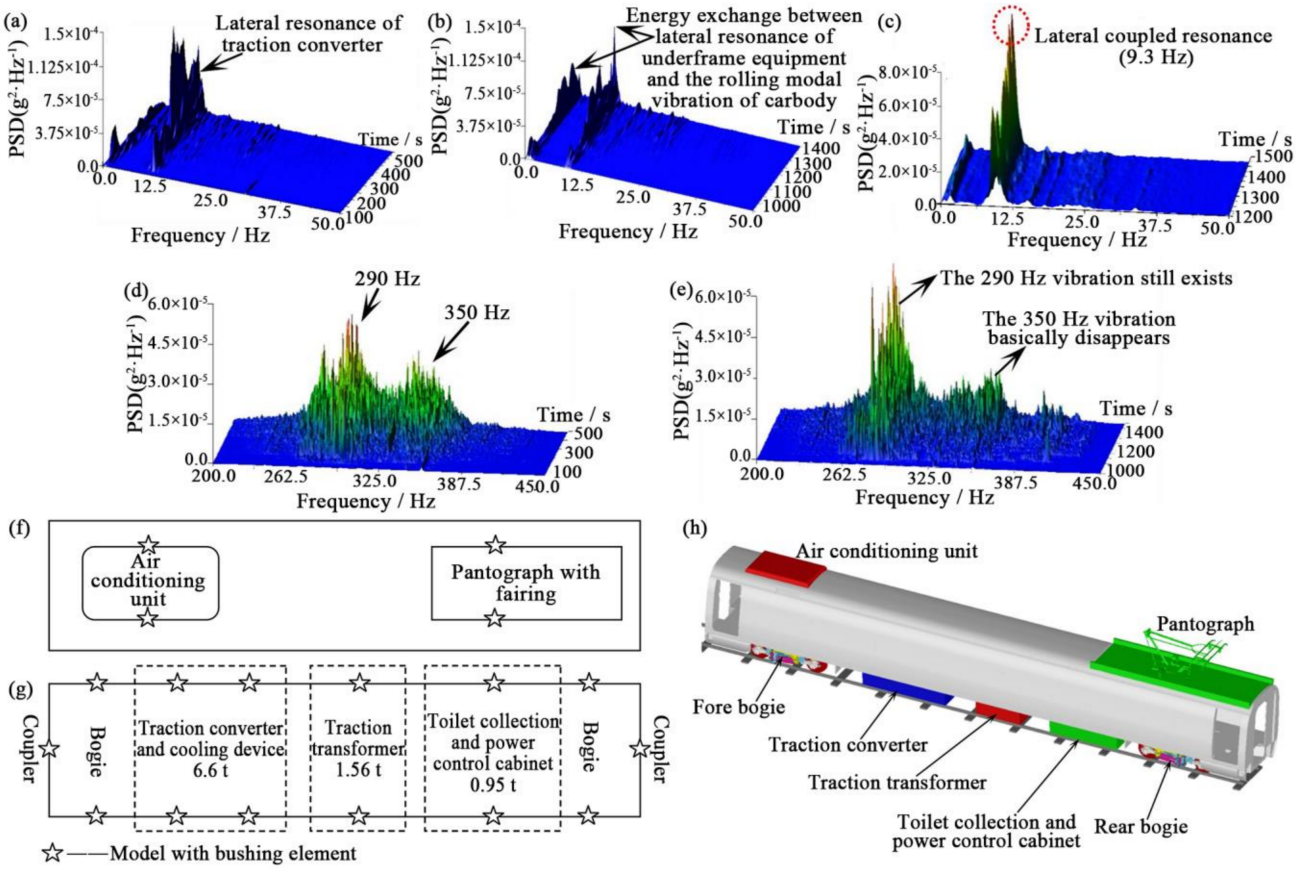

Figure 7. Rigid-flexible coupling simulation model formulation of trailer TC02/07 based on optical fiber test and analysis results of three acceleration PSD contrast for hanging traction converter, as seen in Figure 6f–h, including starting section I from stationary acceleration time history (**a**), starting section II from critical acceleration time history (**b**)and stable section III from critical acceleration time history (**c**); And two acceleration PSD contrast (**d**,**e**) for side beams in floor frame corresponding to (**a**,**b**). Between aluminum alloy car body and the external equipments, two main interfaces are constituted with roof interface (**f**) and floor frame interface (**g**), and rigid-flex coupling model of trailer TC 02/07 (**h**) formulated with weak coupling interface of floor frame so as to ensure 30-year service life.

In order to avoid strong electromagnetic interference, this tracking test adopts the novel technique of optical fibre measuring, and the acceleration sensitivity can reach 1 K Hz. For the floor frame, as shown in Figure 7d,e, both side beams only generate high-frequency elastic vibration with a dominant frequency of ca. 290 Hz since the unsteady aerodynamic load is caused by the skirts with reinforcement design supports. After the self-weight wedge tight failure on some rubber hanging joints, the traction converter reciprocates and moves laterally, and the high-frequency elastic vibration with the dominant frequency of ca. 350 Hz is significantly weakened.

Combined with the analysis results of this tracking test, as shown in Figure 7f–h, the rigid-flex coupling simulation model of trailer TC02/07 was formulated according to the principle of weak coupling interface, and the formation mechanism of internal lateral coupling resonance is fully confirmed by the dynamic simulation analyses [49,50]. However, the new rubber hanging elements were mistakenly used to implement the DVA damping technique. If the impact of repeated roll vibration is excluded, as shown in Figure 8, the lateral acceleration of the traction converter exceeds the limit specified in IEC61373—2010, forcing the self-excited vibration of the middle diamond mode for the service car body. Consequently, the accompanying vibration of roof twisted mode completely exposed the

inherent defects of aluminum alloy car body, as shown in Figure 9, and the construction speed (or design speed) could not be further promoted anymore.

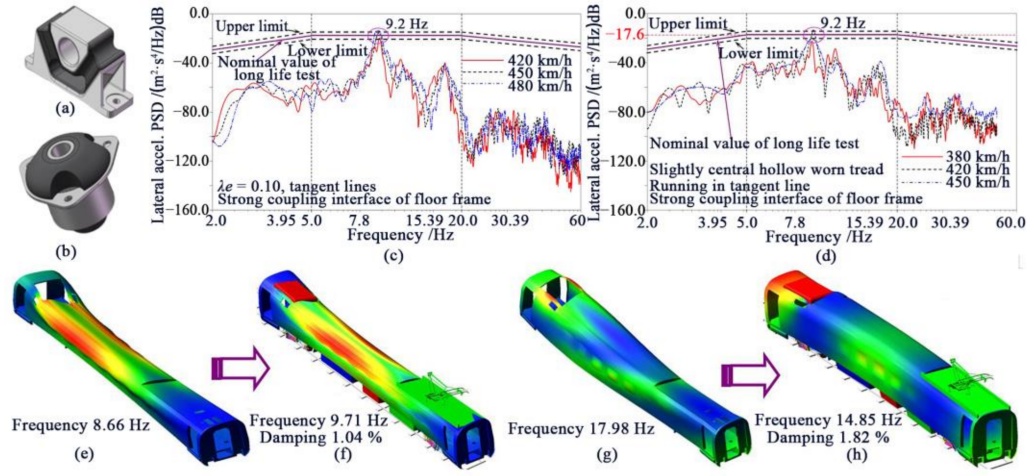

Figure 8. Formulations of strong coupling interface under floor frame of service car body after replacing with new rubber hanging elements. (**a**) New V-type rubber hanging elements for traction converter. (**b**) New Conic rubber hanging elements for traction transformer, toilet collection, etc. (**c**) Lateral acceleration of traction converter exceeds limit specified in IEC61373–2010 when running speed of (420–480) km/h in tangent line at λ_e = 0.10. (**d**) Lateral acceleration exceeds limit again when running speed of (380–420) km/h in tangent line with slight central hollow tread wear. Considering strong coupling interface formulated under floor frame, central rhombus modal frequency of service car body is then increased slightly from inherent 8.66 Hz to 9.71 Hz due to corresponding master-slave node constraints (**e**,**f**), by which lateral coupling relationship is established with acceleration response of bogie frame lateral vibration, causing traction converter to occasionally generate internal coupling resonance. Meanwhile, 1st lateral bending modal frequency of service car body is then decreased from inherent 17.98 Hz to 14.85 Hz due to generalized mass increase (**g**,**h**).

The nonlinear variation in the inner forces of relevant constraints is one of the main reasons for the elastic vibrations of lightweight structures. The vibration fatigue damage assessment based on the master S-N curve of modal structural stress shows that: as shown in Figure 9d,g, the accompanying vibration of roof twisted mode exposes the impacts of crescent notch effects at one side of pantograph on the fatigue lives at both ends of transverse weldline. Specifically, when the vehicle speed is 450 km/h, as shown in Figure 9c, the coupling resonance occurs in the roof twisted mode, and the fatigue life of critical nodes decreases to 545 $\times$ 10^4 km. When increased to 650 km/h, the more intense coupling resonance occurs, and the fatigue life decreases further to 138 $\times$ 10^4 km.

When the impact of repeated roll vibration is considered, the actual situation will become worse e.g., the maximum of lateral/vertical accelerations is 1.4/1.7 g, respectively, due to the unstable vibration of transformer (ca. 1.6 t), and the resonances of the local ceiling interior are caused thereby. As such, the dual coupling interactions of wheel-rail and pantograph-catenary are possible to occur thereby [51].

In terms of the service car body system, shaking and fluttering are two quite different phenomena. The high speed car body shaking phenomenon at low conicity usually refers to the rolls and rocks of service car body caused by the primary hunting design default, i.e., the deficient phase margin of rear bogie yaw or hunting instability. And the unsteady aerodynamic load becomes one of the most important related factors. Line tracking test analyses can confirm: (i) the main frequency is ca. 2.5 Hz for motor vehicle shaking, which is approaching the modal frequency of traction motors swung laterally with hanging frames corresponding to the rear motor bogie; (ii) the main frequency is changed to ca. 1.5 Hz for trailer vehicle shaking, which is determined by the anti-roll nonlinear stiffness.

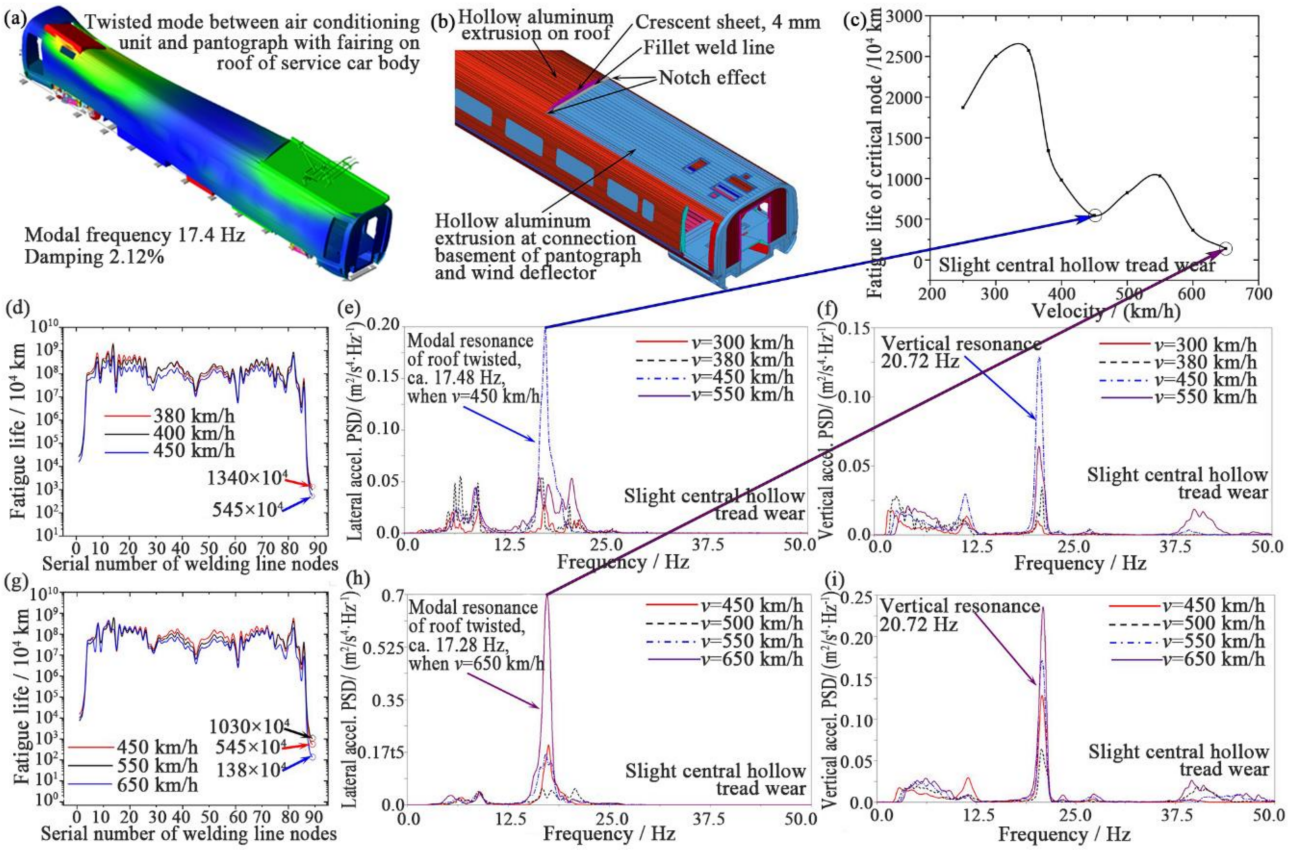

Figure 9. Lateral coupling resonances in equipment cabin under floor frame and associated influences on fatigue damage of aluminum alloy car body. (**a**) Rhombus modal coupling resonance in middle of service car body is accompanied by roof twisted modal vibration, ca. 17.40 Hz. (**b**) Crescent notch effect on one side of pantograph fairing and associated influences on fatigue damage at both ends of transverse weldline. (**c**) Relationship curve of vehicle speed influence on fatigue life at both ends of transverse weldline, in which roof is twisted and resonant when 450 km/h, and stronger resonance occurs again when 650 km/h. (**d**–**f**) Lateral and vertical vibrations of pantograph fairing and associated influences on fatigue life at both ends of transverse weldline when speed of (300–550) km/h. (**g**–**i**) Lateral and vertical vibrations of pantograph fairing and associated influences on fatigue life at both ends of transverse weldline when speed of (450–650) km/h.

4. Next Generation HSRS with Higher Speed

As for the next generation of higher speed HSRS, the self-adaptive improved design of higher speed bogies will take German ICE3 serial bogies as the technical prototype, and the self-adaptive basic idea was put forward and verified in the literature [52,53]. This low-cost solution has been working to perfection constantly in scientifically promoting the limit and construction speeds under the rational condition of wheel-rail matching, by which the large-scale MDO platform can be constituted to achieve the above three goals.

4.1. Self-Adaptive Improved Design of Higher Speed Bogies

In order to overcome the primary hunting design default existing in the prototype of German ICE serial bogies, the analysis graphs of full-vehicle stability properties and variation patterns, as shown in Figure 10, clarify the correct direction of self-adaptive improved design for higher speed bogies, including the main reasons as follows:

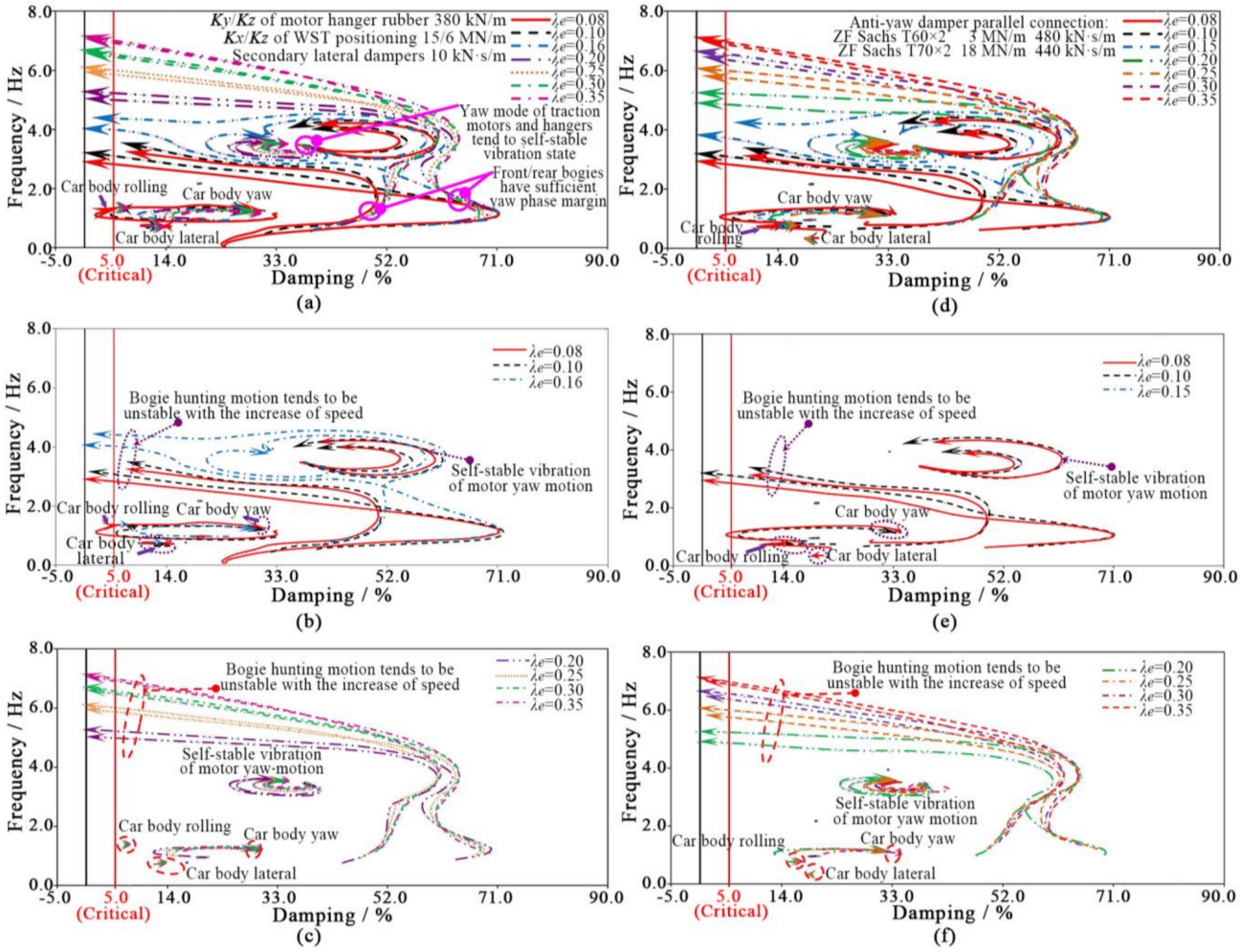

Figure 10. Analysis graphs of stability properties and variation patterns for self-adaptive higher-speed bogie with anti-rolling torsion bar devices (in-) active. (**a**) When λ_e = 0.08–0.35 with anti-rolling torsion bar devices active. (**b**) When λ_e = 0.08–0.16 with anti-rolling torsion bar devices active. (**c**) When λ_e = 0.20–0.35 with anti-rolling torsion bar devices active. (**d**) When λ_e = 0.08–0.35 with anti-rolling torsion bar devices inactive. (**e**) When λ_e = 0.08–0.15 with anti-rolling torsion bar devices inactive. (**f**) When λ_e = 0.20–0.35 with anti-rolling torsion bar devices inactive.

(1) There is a rational matching relationship between wheelset positioning constraint stiffness and anti-hunting dynamic features. Specifically, the longitudinal/lateral stiffness of wheelset positioning is ca. 15/6 MN/m, respectively. So, the novel anti-yaw dampers of ZF Sachs T60 and T70 are combined in parallel to establish the anti-hunting broadband energy-absorbing mechanism.

Special attention: for ZF Sachs T60 × 2, the rating values of linear damping and hydraulic stiffness need to be required to ca. 480 kN·s/m and ca. 3 MN/m; whereas for ZF Sachs T70 × 2, the parameters are the same as the original ones, i.e., ca. 18 MN/m and ca. 440 kN·s/m. The radial stiffness of rubber joints at both ends is ca. 70 MN/m.

(2) In order to avoid the rapid attenuation of the bogie yaw phase margin as much as possible, the lateral/vertical stiffness of motor hanging rubber joints is taken as ca. 380 kN/m, and the effects of detouring flow can be constructed thereby.

Specifically, the lower the actual equivalent conicity, the greater the kinetic energy released in time by the modal vibration of traction motors swung laterally with hanging frames, thus ensuring the hunting motion stabilization. Whereas the actual equivalent conicity is increased, the lateral-swung of traction motors with hanging frames tends to self-stable vibration, thus reducing the wheel-rail dynamic interaction.

(3) Unlike the primary or secondary hunting phenomenon, the simple problem of car body instability is only related to the anti-roll torsion bar device, i.e., the self-excited vibration of car body up-swung or roll mode occurs within the range of vehicle speed (140–200) km/h at $\lambda_e < 0.10$. When the anti-roll torsion bar device is not activated, the above self-excited vibration will be converted into the modal vibration of car body yaw. Therefore, the self-adaptive improved design needs a low-cost solution to remove or eliminate the car body instability.

4.2. Solution to Car Body Instability at Minimum Cost

Combined with the specific application of the outer windshield [54], as shown in Figure 11, the implementation of a semi-active damping technique between inter-vehicles is proposed with the conservation principle of momentum, i.e., the inertia moment of car body yaw is much greater than that of car body roll, I_{zz}>>I_{xx}, At the same time, this technical implementation also avoids cracks in the lower part of the outer windshield on both sides due to slot disturbance effects.

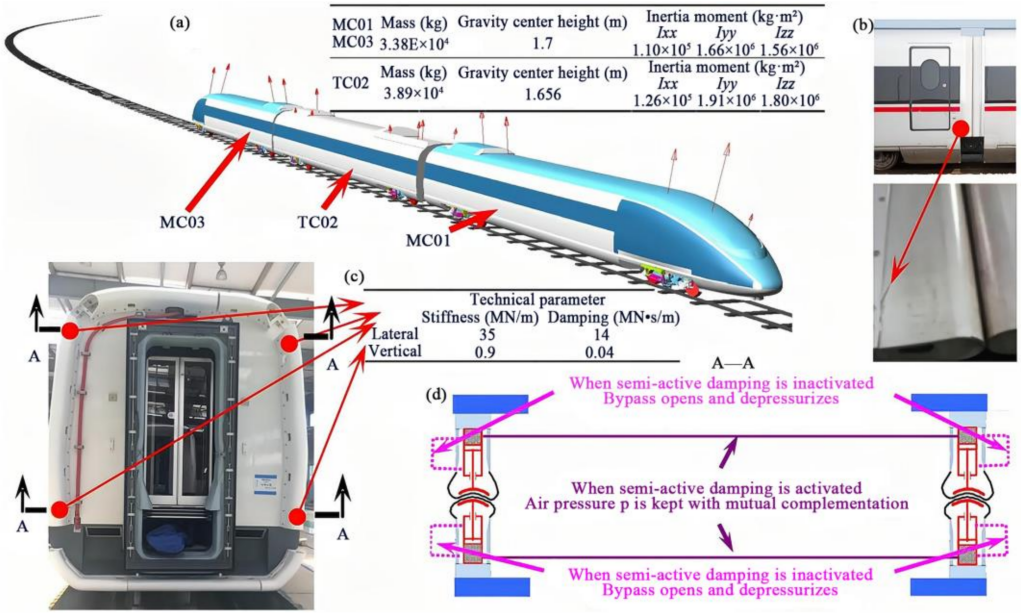

Figure 11. Semi-active damping solutions between inter-vehicles and associated technical implementation. (**a**) Motor-trailer-motor trainset with relevant parameters. (**b**) Cracks occur on lower part of outer windshield at both sides. (**c**) Semi-active damping implementation with stiffness and damping in lateral and vertical directions per constraint point. (**d**) Principles of pneumatic technique when activated or inactivated.

Like the self-adaptive improved design of high-speed bogies with four ZF Sachs T60 per bogie [55], the dynamic simulation of a three-vehicle trainset shown in Figure 11a can also prove that this low-cost solution will improve the influence of car body instability on ride comfort, with the lateral evaluation index $Wz < 2.5$ within the range of vehicle speed (140–200) km/h at $0.03 < \lambda_e \leq 0.10$. Compared with the integrated suspension control solution of car body lateral and roll [40], the semi-active damping technique is technically reliable and easy to maintain between inter-vehicles.

4.3. Comprehensive Assessment of Safety and Stability

By using three different wheel profile designs and the lateral span variations of nominal rolling circles, as shown in Table 2, eight different conditions are constructed for wheel-rail matching. The comprehensive assessment of safety and stability shows that when $\lambda_e < 0.10$, as shown in Figure 12, the hunting motion stabilization will be maintained with

the hypothesis of small creepage and non-spin, which is a sufficient and necessary condition for the formation of the uniform wear stage at low conicity.

Table 2. Influence of actual equivalent conicity on limit speeds of motor and trailer vehicles.

Wheel Profile Typical Design	Lateral Span between Nominal Rolling Circles/mm	Equivalent Conicity/λ_e	Max. Speed for Motor Vehicles/(km/h)	Max. Speed for Trailer Vehicle/(km/h)	Remarks
XP55	1493	0.06	790	740	When v > 200 km/h and λ_e < 0.10, safety speeds under hunting motion stabilization are determined by maximum wheel unloading rate.
LM	1472	0.08	765	——	
LM	1493	0.10	555	650	For motor vehicle, safety speeds are determined as required in UIC518 or EN14363, but for trailer, safety speeds are decided by concept of limit speed. i.e., safety threshold of lateral acceleration of bogie frames can be increased to ca. 1.5 g.
S1002G	1500	0.16	530	600	
S1002G	1504.3	0.20	435	480	
S1002G	1506.1	0.25	405	420	
S1002G	1506.8	0.30	390	390	Safety speeds are determined as required in UIC518 or EN14363.
S1002G	1507.2	0.35	380	380	

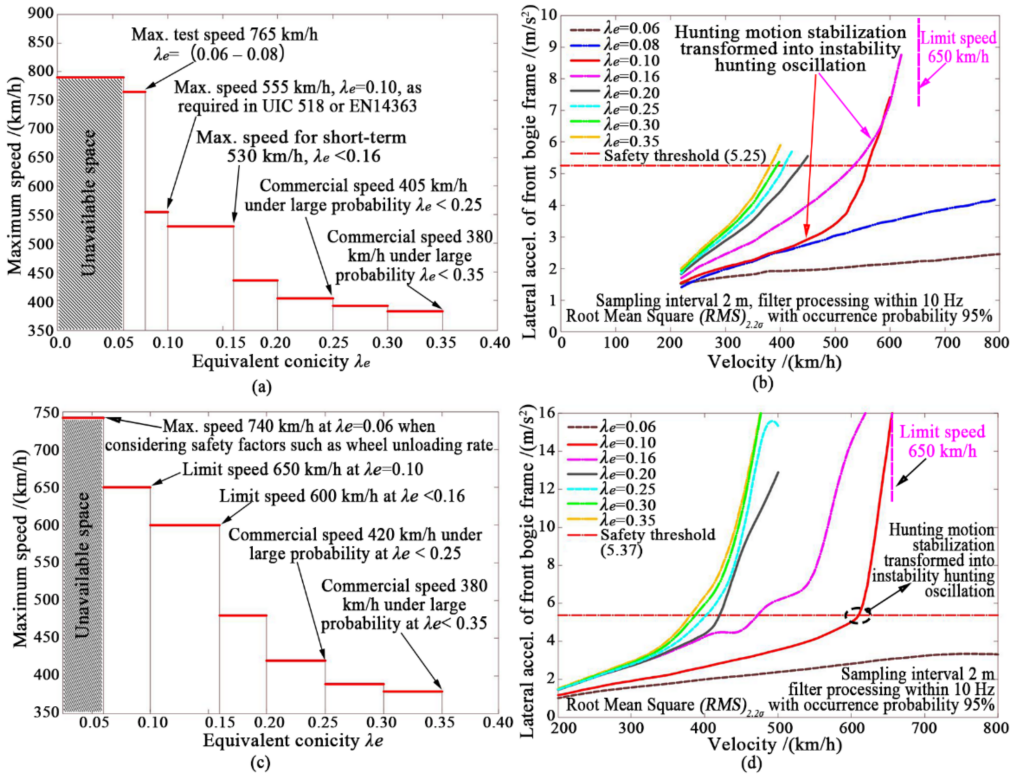

Figure 12. Safety and stability assessments of self-adaptive improved motor and trailer vehicles. (**a**,**b**) Evaluations of safe speed space of motor vehicle and associated lateral acceleration of bogie frame based on UIC518 or EN14363. (**c**,**d**) Evaluations of safe speed space of trailer vehicle and associated lateral acceleration of bogie frame according to concept of limit speed.

However, when λ_e = 0.10/0.16, the hunting motion stabilization is transformed into instability hunting oscillation. For the motor vehicle, according to UIC518 or UIC14363, the maximum speed is allowed to 555/530 km/h. Meanwhile, for trailer vehicles, the maximum speed can be increased to 650/600 km/h if the safety threshold value is set to 1.5 g. So, the self-adaptive improved design of higher speed bogies is able to break the worldwide HSR record of 575 km/h when 0.03 < $\lambda_e \leq$ 0.15. Considering the normal wear of wheel-rail contact and associated effects of tight track gauge, when λ_e = (0.20–0.35), there is little room for promoting the safety speed.

For this reason, the rail experts are reminded that the occurrence probabilities of track conicity (0.03–0.10), 0.25, and 0.35 should be controlled with 85%, 95%, and 99%,

respectively, i.e., the occurrence probability of track conicity (0.25–0.35) is required to be less than 5%.

4.4. Wear Evolution Regulation under Rational Condition of Wheel-Rail Matching

Taking the trailer vehicle as the research project, the normal wear regulation is formed with the nonlinear variation of wheel-rail contact geometry, as shown in Figures 13–15, including the three main stages of uniform wear at low conicity, rapid wear evolution, and stable wear at high conicity.

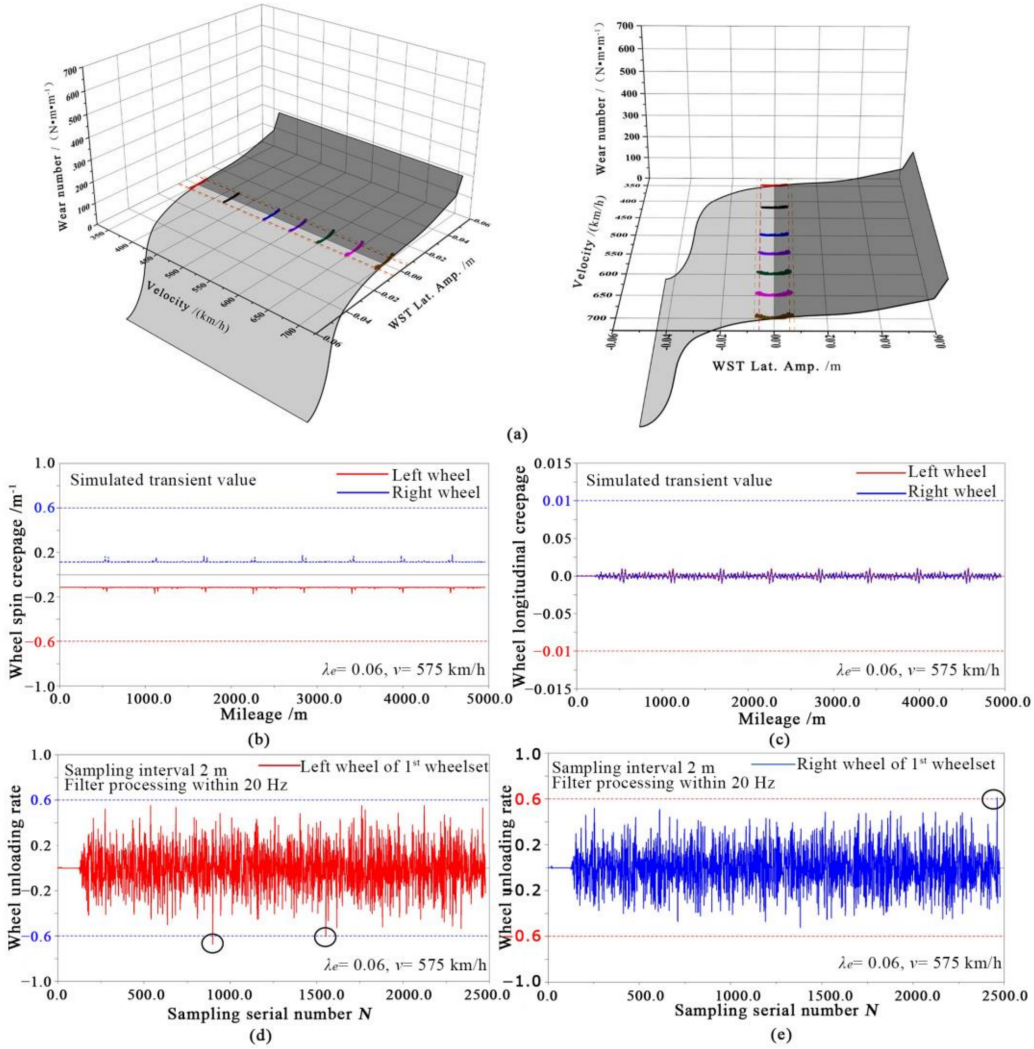

Figure 13. Hunting motion stabilization at low conicity of λ_e = 0.06 when running in tangent lines. (**a**) Influence of vehicle speed increase on distribution characteristics of wheel wear index. (**b**,**c**) Variation patterns of wheel spin and longitudinal creepage when running at 575 km/h, which is maintained with the hypothesis of small creepage and non-spin. (**d**,**e**) Left and right wheel unloading rates of 1st wheelset when running at 575 km/h, the maximum value 0.60 has small occurrence probability of ≤5%.

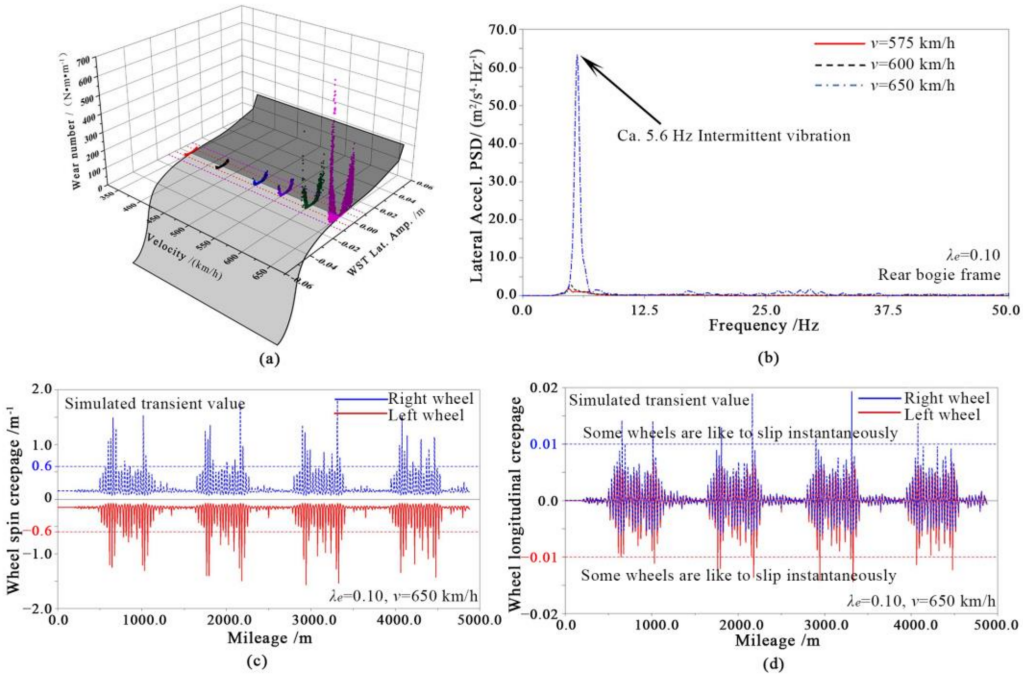

Figure 14. Concept of limit speed explained as suddenly transition from hunting motion stability to instability hunting oscillation at λ_e = 0.10, which becomes High Creepage Issue. (**a**) Influence of vehicle speed on distribution characteristics of wheel wear index in tangent line operations. (**b**) Lateral acceleration PSD of rear bogie frame changes suddenly into forced resonance, ca. 5.6 Hz, when v = 650 km/h. (**c**,**d**) High Creepage Issue represented through variation patterns of wheel spin and longitudinal creepage for left and right wheels of 1st wheelset.

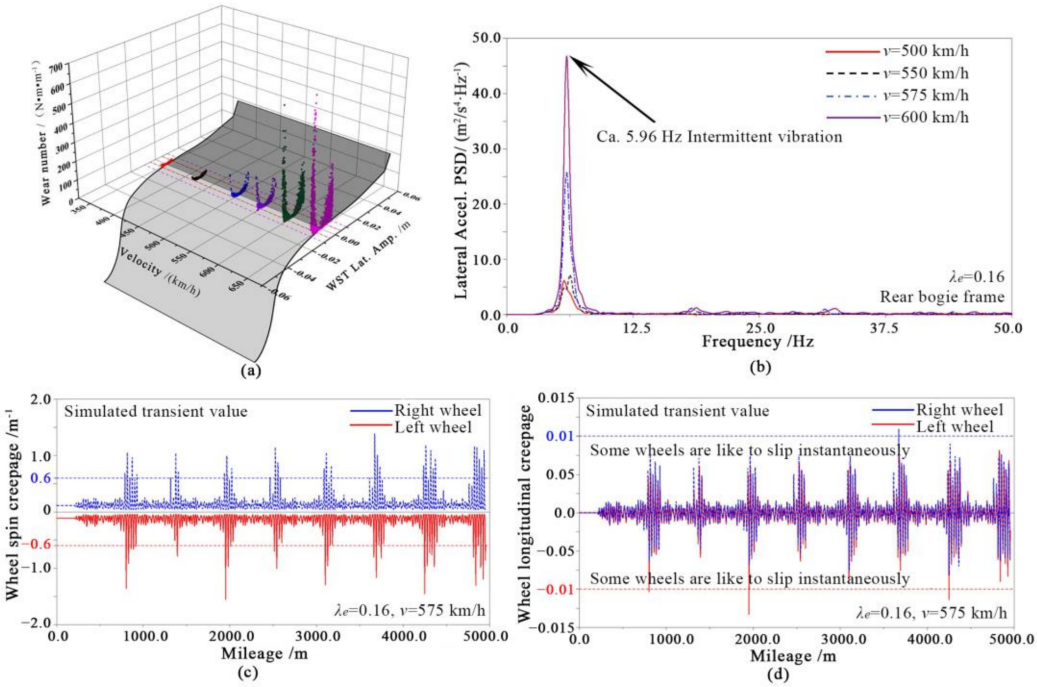

Figure 15. Gradual transition from hunting motion stability to instability hunting oscillation at λ_e = 0.16. (**a**) Influence of vehicle speed on distribution characteristics of wheel wear index in tangent line operations. (**b**) Lateral acceleration PSD of rear bogie frame changes gradually into forced resonance, ca. 6.0 Hz, when v = 600 km/h. (**c**,**d**) Variation patterns of wheel spin and longitudinal creepage, which is one of main characteristics of stable wear stage at high conicity.

(1) Uniform wear at low conicity. Under the collaborative and innovative efforts between vehicle and rail disciplines, the self-adaptive improved design of higher speed bogies returns to the rational condition of wheel-rail matching, i.e., λ_{emin} = (0.03–0.06), as shown in Figure 13, and the uniform wear stage at low conicity will bring considerable cost effectiveness to Chinese HSR practices.

These beneficial findings are mainly manifested in the following three aspects: (i) When running in tangent lines or in a large radius curving negotiations, as shown in Figure 13a, the low wear area becomes wider and the amplitude of wheelset hunting motion increases correspondingly; (ii) The hypothesis of small creepage and non-spin is valid, by which the stability robustness performance can be gained against aerodynamic disturbances such as crosswind, sidewind, or wake, as shown in Figure 13b,c; (iii) Because the rubber pad and pressing buckle are the only damping elements for ballastless track bed with seamless rails, when approaching the limit speed, as shown in Figure 13d,e, the maximum rate > 0.60 of wheel unloading becomes a small occurrence probability event of $\leq$0.15%.

These findings once again demonstrate that the rational condition of wheel-rail matching cannot be easily abandoned, which is one of the necessary conditions for the successful commercial applications of HSRS in the high-tech manufacturing industry. This rational condition is unique to Chinese HSR parameter system, which does not require the improved design of the wheel-rail relationship, such as rail grinding treatment or wheel profile renewal design. However, as a classic research case of large-scale MDO, HSRS must emphasize the significance of actively recommending and introducing the dynamic design methodology, in which the analysis graph of full-vehicle stability properties and variation patterns becomes one of the key technologies. As a result, the correct direction of self-adaptive improved design is clarified for higher-speed bogies by using PODA.

(2) Rapid wear evolutions due to wheel spin singularities. According to the duality of hunting kinematics and dynamics, as shown in Figure 14, the critical rapid evolutions are constructed in commercial HSR practices. That is to say, the wheel-rail contact of HSR has a dialectical relationship between (near-) linearity and nonlinearity. Wickens cited the wheel spin to better explain the geometric nonlinear impacts of wheel-rail contact. To this end, a broader MDO technical platform should be built together with the experts in vehicle, rail, passenger transport, etc.

When λ_e = 0.10, as shown in Figures 12b,d and 14a, the very evident transition characteristics can be seen between hunting motion stabilization and instability hunting oscillation, i.e., the wear indices at both ends are curled up due to wheel spin increase. This kind of transition characteristic has uncertain influencing factors, such as aerodynamic loading excitations. For instance, when operating on mountain lines with bridges and tunnels accounting for more than 90%, open and dark lines are staggered, or trains are passing each other on elevated rails, etc. Because the primary hunting design default exists in the prototype of ICE3 serial bogies, the above kind of transition characteristics will appear in advance, so that the central hollow tread wear will inevitably become a large probability event due to the long-term operations on dedicated lines.

Compared with the concept of critical speed, as shown in Figure 14, limit speed has a clearer intention and extension. If the safety threshold is raised to ca. 1.5 g and the vehicle speed is close to 650 km/h, the trailer bogie frame will suddenly have a very strong lateral resonance. When the maximum value of wheel spin creepage exceeds 0.60, the maximum value of wheel longitudinal creepage is greater than 0.01. Consequently, the wheel will slip instantaneously, and the flat scar wheel may be gradually formed thereby. Most scholars believe that the flat scar wheel is likely to become one of the direct inducements for the longitudinal uneven wear formation of wheel-rail rolling contact.

When approaching the limit speed of 650 km/h, special attention should be paid to the changes in the rubber node load of the rotary arm axlebox, such as a sharp increase in the maximum amplitude of longitudinal cyclic loads.

Relatively speaking, considering the primary hunting phenomenon that existed in the German ICE3 prototype, the limit speed will be reduced to ca. 480 km/h or a little higher, which is the main reason why the central hollow tread wear has become an exclusive event with a large occurrence probability in the duration of the long-term operations on dedicated lines.

(3) Stable wear at high conicity with tight track gauge effects. When λ_e = 0.16, as shown in Figure 15, the negative influences of wheel spin creepage on instability hunting oscillations are enhanced to some extent. Furthermore, the trailer bogie frame will also have a similar process of gradual-enhanced lateral resonances due to the tight track gauge effects.

When λ_e > 0.16, as shown in Figure 12b,d, the tight track gauge effects will grow stronger so that the instability hunting oscillation becomes the dominant behavior, resulting in the terrible problems of wheel-rail dynamic interaction and noises. For this purpose, the collaborative and innovative efforts of rail professionals are required, such as preventive or maintenance rail grinding treatments to avoid the RCF failure on the rail shoulder at one side of the gauge corner as much as possible.

4.5. Design Optimization of Service Car Body System

In order to ensure the 30-year service life of the aluminum alloy car body, as shown in Figures 16–18, the passenger transport discipline should carry out optimal route planning and design so as to remove and eliminate the negative impacts of central hollow tread wear on the lateral coupling vibration of the service car body.

(1) External excitation source belongs to unsaturated and unsteady state. As shown in Figure 16, a mutual influence will occasionally take place between the parametric disturbance of wheel spin and the forced vibration of the bogie frame. As for slight central hollow tread wear, the local conformal or bad contact is occasionally constructed on specific rail sections, the rail running light band becomes widened, and the wheel wear is concentrated on the central tread. Different from the bogie hunting instability failure caused by the primary or secondary hunting phenomenon, the slight central hollow tread wear forces the wheels to produce spin creepage. As a result, the wheelsets produce a small-amplitude instability hunting oscillation, and the bogie frame has a forced vibration response, which is not the modal vibration of bogie frame lateral or yaw motion.

This forced vibration response can only change into resonance when the vehicle speed is greater than 450 km/h, the dominant frequency of which changes to ca. 6.0 Hz. Therefore, within the service speed of (300–450) km/h, the above forced vibration response has obvious broadband characteristics, with the dominant frequency of ca. (7.0–8.0) Hz and the leading frequency of 10 Hz or more in general, which constructs a sufficiently strong external excitation source. Specifically, in the general curving negotiation with a speed of 250 km/h, the UK small defect spectrum does not change the wear characteristics shown in Figure 16c.

In order to avoid the further deterioration of such forced vibration responses, it is necessary for the passenger transport discipline to carry out the planning and design optimization of the operating routes, as shown in Figure 17, to enhance the self-cleaning capability of central hollow tread wear. The German track spectrum of high interference does not weaken the excitation inputs for small defects of wavelength $\leq$3 m and long-wave irregularities. Especially, the long-wave horizontal irregularity excitation input can cause the roll and rock of service car body.

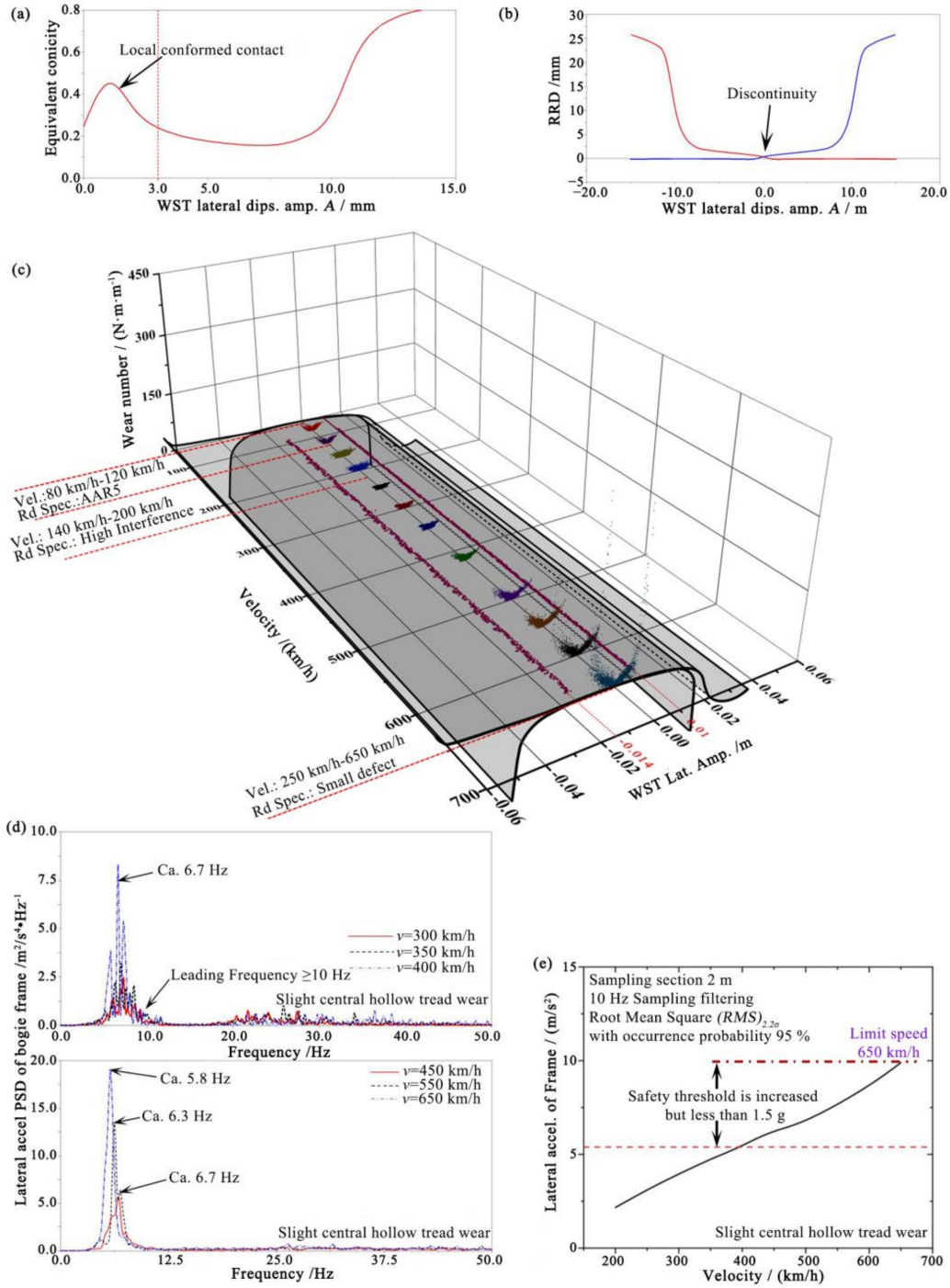

Figure 16. Central hollow tread wear results occasionally in local conformal or bad contact between worn wheel and rail on some rail sections, which forces bogie frame to produce lateral forced vibration when running in tangent lines. (**a**,**b**) Equivalent conicity and RRD curves calculated by slight central hollow tread wear. (**c**) Travelling wide light band is formed on top surface of railhead while concentrated wear is evolved on wheel tread. (**d**) Bogie frame thereby generates forced resonance with dominant frequency of ca. 6 Hz and leading frequency is close to or more than 10 Hz. (**e**) Influence of vehicle speed on lateral acceleration $(RMS)_{2.2\sigma}$ of bogie frame.

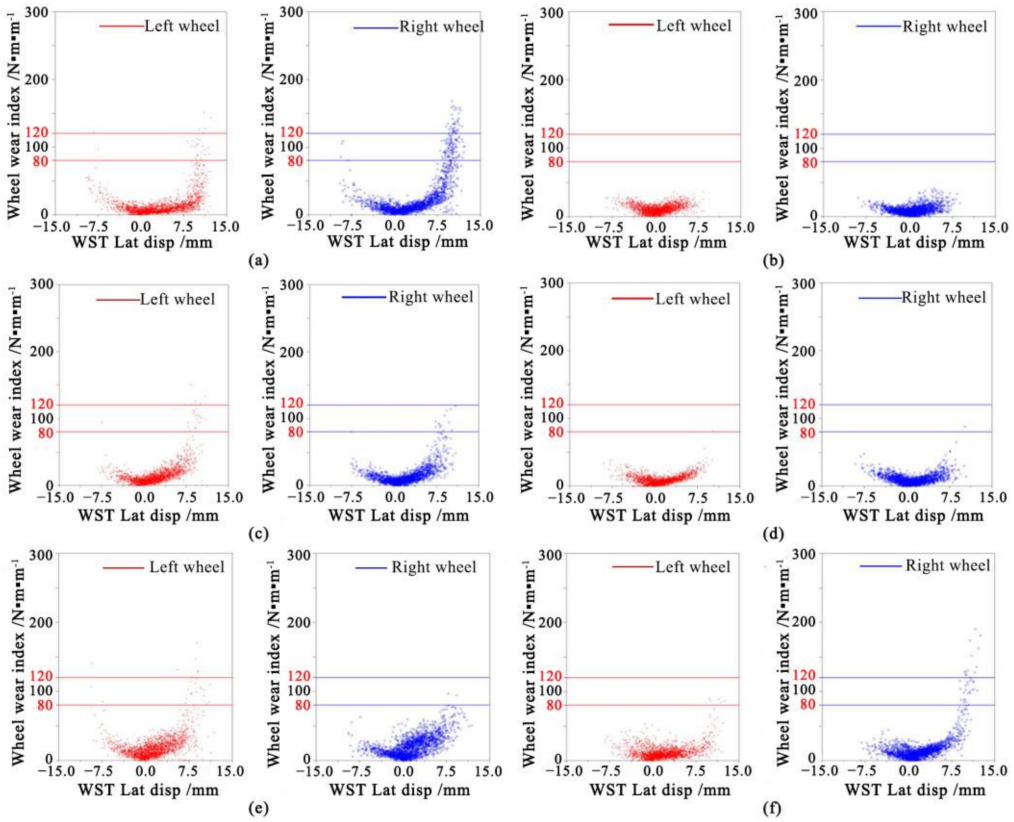

Figure 17. Self-cleaning of central hollow tread wear can be verified when M-T-M three-car trainset across over dedicated lines of 200 km/h grade, running at 200 km/h in curving negotiation with radius 3000 m, superelevation 150 mm and transition (500–700) m. (**a**,**b**) Distribution characteristics of left and right wheel wear index for 1st and 4th wheelsets of front motor vehicle. (**c**,**d**) Distribution characteristics of left and right wheel wear index for 1st and 4th wheelsets of middle trailer vehicle. (**e**,**f**) Distribution characteristics of left and right wheel wear index for 1st and 4th wheelsets of rear motor vehicle.

(2) Correlative excitations come from internal lateral resonances. By applying MMRT, the transaction strategy of the flexible body-to-MBS interface was improved, as shown in Figure 18, so as to remove and eliminate completely the lateral coupling relationship between running gear and the service car body.

As mentioned above, through the collaborative and innovative efforts of vehicle, rail, and passenger transport disciplines, the slight central hollow tread wear provides the necessary conditions for the structural experts to better realize the structural dynamic response design optimization of an aluminum alloy car body. In order to ensure a weak coupling interface, the independent design of the equipment cabin under the floor frame mainly includes the following three points:

(1) In order to avoid the negative impacts caused by the reciprocating lateral movement of the traction converter, e.g., skirt plate bracket cracks or bolt connection failure (loosed or broken), it is necessary to use the novel rubber hanging elements; as shown in Figure 8a,b, the proportional damping is set as (0.3–0.5)% for elastomers.

(2) However, the necessary measures, such as bolt pre-tightening or self-weight wedge tightening, must be taken to raise the vertical hanging stiffness as much as possible so as to avoid the accompanying vibration of the traction converter and other equipment rolling repeatedly.

(3) Since the traction converter has the largest generalized mass, the lateral modal frequency is the lowest. For this reason, the structural experts should manage the weak coupling interface, trying their best to raise the lateral modal frequency of the traction

converter to ca. 14 Hz. And the lateral modal frequency of other hanging equipment (m < 1250 kg) shall not be less than 12 Hz.

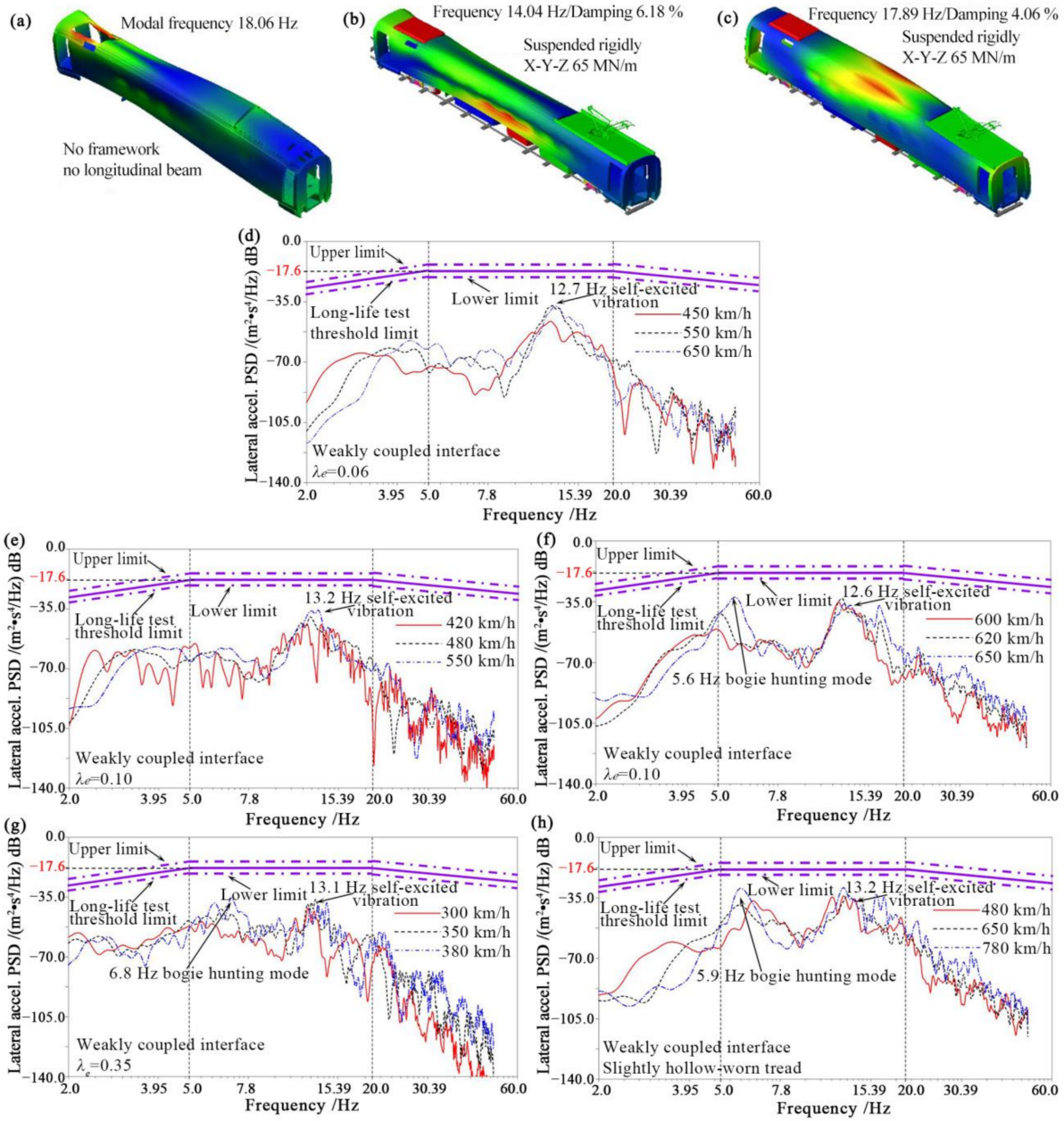

Figure 18. Optimization design of rubber hanging parameters for equipment cabin under floor frame based on weak coupling interface is adopted for service car body system, so as to avoid internal lateral coupling resonance of traction converter as much as possible. (**a**–**c**) 1st order lateral bending inherent mode of aluminium alloy car body has evolved into two critical modes, i.e., 1st order lateral bending modes on lower and upper parts of service car body. (**d**) Safety assessment of lateral vibration for traction converter when running in a tangent line approaching to limit speed of 650 km/h under λ_e = 0.06 according to specified in IEC61373—2010. (**e**,**f**) Safety assessment of lateral vibration for traction converter when running in a tangent line with higher speeds of (420–550) km/h and near to limit speed of 650 km/h under λ_e = 0.10. (**g**) Safety assessment of lateral vibration for traction converter when running in a tangent line with service speeds of (300–380) km/h under λ_e = 0.35. (**h**) Safety assessment of lateral vibration for traction converter when running in a tangent line with three speed grades of 480/650/780 km/h when considering negative impacts of detrimental wear like central hollow tread wear.

The independent design of the above equipment cabin is based on the following two guidelines to realize the weak coupling interface:

(1) The improved transaction strategy of the flexible body to MBS interface is implemented by applying MMRT. Specifically, considering the low dynamic interaction requirements of both interfaces, including the floor frame under which equipment such as the traction converter is hanged and the roof on which the pantograph with fairing and the air conditioning unit are installed, the constrained DoF is set to zero.

(2) As shown in Figure 18a–c, the 1st lateral bending inherent mode of the aluminum alloy car body is transformed into the 1st lateral bending modes of the service car body on the lower/upper parts; both modal frequencies are ca. 14.0/17.9 Hz.

As shown in Formula (22), only when the constraint DoF is zero will the corresponding interface stiffness be enhanced and the relevant modal mass be reduced. That is to say, under the strong coupling interface, the central rhombus modal frequency of the service car body is ca. 9.7 Hz, which becomes the critical modal vibration. Meanwhile, under the weak coupling interface, it changes into the 1st lateral bending mode on the lower part, ca. 14.0 Hz. So, the lateral coupling relationship is then removed between the running gear and the service car body.

According to the provisions of IEC61373–2010, as shown in Figure 18d–h, the simulation analyses of various working conditions show that the traction converter has no lateral coupling resonance and is far below the safety threshold. According to the floating plate effect, the moderate lateral vibration of the traction converter releases the corresponding kinetic energy in time, which is beneficial to maintaining the ESL safety of the aluminum alloy car body. From this, it can be seen that the optimization design of rubber hanging parameters in the equipment cabin under the floor frame also has a horizontal DVA effect similar to that of high-rise buildings.

At the same time, it is also confirmed again that the self-adaptive improved design for the next generation HSRS can satisfy the higher speed requirements. If the safety threshold of bogie vibration early warning can be raised to 1.5 g when the actual equivalent conicity is limited to the following range, i.e., $0.03 < \lambda_e < 0.15$, the higher speed self-adaptive improved design has the technical capacity to break the worldwide record of 575 km/h, so as to optimize the repair class and repair system with operation and maintenance cost minimization.

In general, the dynamic design methodology should be recommended and introduced in high-tech manufacturing industries such as HSRS, grasping firmly the nonlinear influencing factors of the main interfaces with appropriate modeling methods. Especially PODA and MMRT are taken as effective tools for big data mining, which can be used to better realize the weak coupling interfaces between different disciplines. Therefore, the successful commercial application of high-tech manufacturing industries such as HSRS requires the support of the MDO technical platform.

5. Conclusions and Prospection

The dynamic design methodology should be actively recommended and introduced to the high-tech manufacturing industries, such as HSRS, so that the development of large-scale complex nonlinear dynamic systems becomes one of its basic works. Moreover, PODA and MMRT are used as effective tools for big data mining to remove and eliminate the singularities of complex constraints and their negative impacts on related interfaces. The following two criteria must be addressed clearly: (i) proper modeling needs to pay very much attention to the premise for investigating engineering problems, e.g., singularity of complex constraints; (ii) the transaction strategy of the flexible body to MBS interface is very crucial, which is closely related to the ESL safety of lightweight structures. In short, no matter what causes the roll and rock of the service car body, it will lead to the improper use of anti-roll torsion bar devices, which has become one of the most common technical problems. Consequently, the central hollow tread wear is then the highest probability event in Chinese HSR practices, with almost no flange root wear or flange side wear. On

the first fluttering phenomenon of the service car body, the contrastive analyses of line tracking tests and rigid-flex coupling simulations show that stability, wear, and vibration are closely related to each other, and the internal lateral coupling resonance of such a traction converter has been one of the main restrictive factors that determine the operation and maintenance costs. With the technical support of relevant analysis software, this paper proposes a large-scale MDO flow chart for HSRS. After defining the key problems to be solved, the self-adaptive improved design solution and associated technical features were formulated and verified for the next-generation HSRS with higher speed requirements.

Through these works on paper, three main conclusions can be drawn as follows:

(1) Only under the rational conditions of wheel-rail matching can the limit and construction speeds be scientifically promoted. By referring to relevant experiences at home and abroad, the rational condition of wheel-rail matching can be determined as follows: $0.10 \geq \lambda_{eN} > \lambda_{emin}$ and λ_{emin} = (0.03–0.06), which is taken as one of the necessary conditions to establish the large-scale MDO technical platform.

(2) Compared with the improved design of the wheel-rail relationship for HSR, the self-adaptive improved design of higher speed bogies is one of the more preferable options. The comprehensive evaluation shows that this self-adaptive improved design solution can solve the car body instability problem at a low cost according to the principle of momentum conservation, making Chinese HSR come back to the rational conditions of wheel-rail matching. By contrast, the steel rail profession unilaterally initiated the improved design of the wheel-rail relationship for Chinese HSR practices, which can neither achieve the uniform wear stage at low conicity nor obtain the stable wear stage at high conicity. For the running mileage of ca. 20×10^4 km only left thereby, Chinese HSR practices prove that the λ_e variation from 0.10 to 0.35 has so many uncertain factors, e.g., service car body shaking phenomenon occurs when high speed running at low conicity of λ_e < (0.10–0.12), or more serious fluttering phenomenon takes place when λ_e is approaching to (0.30–0.35). This is one of the radical reasons for the high costs of Chinese HSR operations and maintenance.

(3) The successful commercial application of high-tech manufacturing industries such as HSRS requires the support of the MDO technical platform. However, the dynamic design methodology plays an active role in developing the large-scale complex nonlinear dynamic system, leading and steering the system design in a more preferable direction, i.e., a self-adaptive, improved design solution for higher speed bogies. This low-cost solution can achieve the following MDO goals: (i) With the cooperation of the rail experts, the occurrence probabilities of track conicity (0.03–0.10) and (0.25–0.35) should be controlled with 85% and 5%, respectively, so that the uniform wear stage can be acquired at low conicity; (ii) Due to λ_{emin} = (0.03–0.06), the passenger transport discipline can carry out the optimal routing planning to realize in time the self-cleaning of central hollow tread wear; (iii) Since the limit speed reaches ca. 650 km/h at λ_e = 0.10, the vehicle specialty can further explore the regulations of higher speed behaviors, to optimize the repair class and repair system and make investment benefit maximization.

According to the new findings from the comprehensive evaluation of the self-adaptive improved design of next generation HSRS, e.g., the limit speed of 650 km/h achieved at λ_e = 0.10 and the self-cleaning mechanism of detrimental wear when operating across different dedicated lines, the running gear needs to further carry out the following two aspects of safety evaluations: (i) Comparative investigations on combination and independent suspensions of traction motors; (ii) analyses and assessments on load safety of the bogie frame and associated rubber joints of the rotary arm axlebox.

Author Contributions: Methodology, M.-W.P.; Validation, C.-G.N. and P.D.; Formal analysis, S.-Y.P., Q.-Z.L. and Y.-N.T.; Investigation, W.D., S.-Y.P., P.D. and Y.-N.T.; Data curation, W.D., C.-G.N., P.D., Q.-Z.L. and Y.-N.T.; Writing—original draft, W.D.; Writing—review & editing, M.-W.P., S.-Y.P. and Q.-Z.L.; Funding acquisition, M.-W.P. All authors have read and agreed to the published version of the manuscript.

Funding: This research is supported by the National key R&D program of China (Grant nos. 2018YFB1201703, 2017YFB0304605, and 2020YFB1200200ZL) and the Research Project of National Innovation Center of High-Speed Train [Grant nos. CXKY-02-01-02(2020)].

Institutional Review Board Statement: Not applicable.

Informed Consent Statement: Not applicable.

Data Availability Statement: Not applicable.

Conflicts of Interest: The author declares no conflict of interest.

References

1. Negrut, D.; Ortiz, J.L. A practical approach for the linearization of the constrained multibody dynamics equations. *J. Comput. Nonlin. Dyn.* **2006**, *1*, 230–239. [CrossRef]
2. Dopico, D.; Gonzaelez, F.; Cuadrado, J.; Kövecses, J. Determination of holonomic and nonholonomic constraint reactions in an index-3 augmentation Lagrangian formulation with velocity and acceleration projections. *J. Comput. Nonlin. Dyn.* **2014**, *9*, 041006. [CrossRef]
3. Allison, J.T.; Herber, D.R. Multidisciplinary design optimization of dynamic engineering systems. *AIAA J.* **2014**, *52*, 691–710. [CrossRef]
4. Wickens, A.H. *Fundamentals of Rail Vehicle Dynamics*; Swets & Zeitlinger: Lisse, Netherlands, 2003.
5. Knothe, K.; Stichel, S. *Rail Vehicle Dynamics*; Springer: New York, NY, USA, 2017.
6. Schiehlen, W. On the history of lateral ground vehicle motions from a multibody dynamics view. *J. Comput. Nonlin. Dyn.* **2015**, *10*, 031014. [CrossRef]
7. Oskar, W. Review of past developments in multibody system dynamics at DLR—From FADYNA to SIMPACK. *Veh. Sys. Dyn.* **2004**, *41*, 339–348. [CrossRef]
8. True, H.; Engsig-Karup, A.; Bigoni, D. On the numerical and computational aspects of non-smoothnesses that occur in railway vehicle dynamics. *Math. Comput. Simulat.* **2013**, *95*, 78–97. [CrossRef]
9. Zeng, X.; Shi, H.; Wu, H. Nonlinear dynamic responses of high-speed railway vehicles under combined self-excitation and forced excitation considering the influence of unsteady aerodynamic loads. *Nonlinear Dyn.* **2021**, *105*, 3025–3060. [CrossRef]
10. Umemoto, J.; Yabuno, H. Parametric and self-excited oscillation produced in railway wheelset due to mass imbalance and large wheel tread angle. *Nonlinear Dyn.* **2023**, *111*, 4087–4106. [CrossRef]
11. Gan, F.; Dai, H.Y.; Gao, H.; Chi, M.R. Wheel-rail contact relationship calculation of worn LMA tread. In Proceedings of the International Conference on Mechanics & Civil Engineering, Wuhan, China, 13–14 December 2014. [CrossRef]
12. Hou, M.; Hu, X.; Li, H. Study on the longitudinal-vertical coupling vibration of high-speed vehicle based on newmark-β forecast-correction integral method. *China Railw. Sci.* **2018**, *39*, 57–62. [CrossRef]
13. Tomioka, T.; Takigami, T.; Fukuyama, A.; Suzuki, T. Prevention of carbody vibration of railway vehicles induced by imbalanced wheelsets with displacement-dependent rubber bush. *J. Mech. Syst. Transp. Logist.* **2010**, *3*, 131–142. [CrossRef]
14. Bokaeian, V.; Rezvani, M.A.; Arcos, R. Nonlinear impact of traction rod on the dynamics of a high-speed rail vehicle carbody. *J. Mech. Sci. Technol.* **2020**, *34*, 4989–5003. [CrossRef]
15. Sayed, M.; Kamel, M. 1:2 and 1:3 internal resonance active absorber for non-linear vibrating system. *Appl. Math. Model.* **2012**, *36*, 310–332. [CrossRef]
16. Preumont, A. Twelve lectures on structural dynamics series. In *Solid Mechanics and Its Applications*; Barber, J., Klarbring, A., Eds.; Springer: Berlin, Germany, 2013; p. 198. [CrossRef]
17. Yang, J. Studies and applications on dynamical design methodology of bogie and rigid-flex coupling simulation for full-assembled vehicle. Ph.D. Thesis, Dalian Jiaotong University, Dalian, China, 2018.
18. Stolpe, M.; Verbart, A.; Rojas-Labanda, S. The equivalent static loads method for structural optimization does not in general generate optimal designs. *Struct. Multidisc. Optim.* **2018**, *58*, 139–154. [CrossRef]
19. Stolpe, M. On the equivalent static loads approach for dynamic response structural optimization. *Struct. Multidisc. Optim.* **2014**, *50*, 921–926. [CrossRef]
20. Koutsovasilis, P.; Quarz, V.; Beitelschmidt, M. Standard input data for FEM-MBS coupling: Importing alternative model reduction methods into SIMPACK. *Math. Comp. Model. Dyn.* **2009**, *15*, 51–68. [CrossRef]
21. Stichel, S. The influence of underframe structural flexibility on the hunting behaviour of a freight wagon. In *Computers in Railways VII*; WIT Press: Southampton, UK, 2000; ISBN 1-85312-826-0. Available online: www.witpress.com (accessed on 12 June 2022).
22. Milovanović, V.; Dunić, V.; Rakić, D.; Živković, M. Identification causes of cracking on the underframe of wagon for containers transportation—Fatigue strength assessment of wagon welded joints. *Eng. Fail. Anal.* **2013**, *31*, 118–131. [CrossRef]
23. Jeong, S.; Shimoyama, K. Review of data mining for multi-disciplinary design optimization. *Proc. Inst. Mech. Eng. Part G J. Aerosp. Eng.* **2011**, *225*, 469–479. [CrossRef]
24. Hiwa, S.; Hiroyasu, T.; Miki, M. Design mode analysis of pareto solution set for decision-making support. *J. Appl. Math.* **2014**, 520209. [CrossRef]

25. Oyama, A.; Nonomura, T.; Fujii, K. Data mining of Pareto-optimal transonic airfoil shapes using proper orthogonal decomposition. *J. Aircraft* **2010**, *47*, 1756–1762. [CrossRef]
26. Marinone, T.; Avitabile, P.; Foley, J.R.; Wolfson, J. Efficient computational nonlinear dynamic analysis using modal modification response technique. In *Topics in Nonlinear Dynamics*; Conference Proceedings of the Society for Experimental Mechanics Series; Adams, D., Kerschen, G., Carrella, A., Eds.; Springer: New York, NY, USA, 2012. [CrossRef]
27. Krack, M.; Scheidt, P.V.; Wallaschek, J. A method for nonlinear modal analysis and synthesis: Application to harmonically forced and self-excited mechanical systems. *J. Sound Vib.* **2013**, *332*, 6798–6814. [CrossRef]
28. Oyama, A.; Fujii, K.; Shimoyama, K.; Liou, M. Pareto-optimality-based constraint-handling technique and its application to compressor design. In Proceedings of the 17th AIAA Computational Fluid Dynamics Conference, Toronto, ON, Canada, 6–9 June 2005. [CrossRef]
29. Silva, R.; Ribeiro, D.; Bragança, C.; Costa, C.; Arêde, A.; Calçada, R. Model updating of a freight wagon based on dynamic tests under different loading scenarios. *Appl. Sci.* **2021**, *11*, 10691. [CrossRef]
30. Ribeiro, D.; Bragança, C.; Costa, C.; Jorge, P.; Silva, R.; Arêde, A.; Calçada, R. Calibration of the numerical model of a freight railway vehicle based on experimental modal parameters. *Structures* **2022**, *38*, 108–122. [CrossRef]
31. Zhang, Y.; Lin, J. *Fundamentals of Structural Dynamics*; Dalian University of Technology Press: Dalian, China, 2007.
32. Castanier, M.; Tan, Y.; Pierre, C. Characteristic constraint modes for component mode synthesis. *AIAA J.* **2001**, *39*, 1182–1187. [CrossRef]
33. Zhan, K. *Robust Design Optimization of Structures under Uncertainties*; Shaker Verlag: Aachen, Germany, 2005.
34. Piao, S.Y. Structural Dynamic Modelling and Frequency-Domain Response Prediction of Launch Vehicles. Ph.D. Thesis, Dalian University of Technology, Dalian, China, 2022.
35. Dong, P.; Hong, J.; Dean, S. A robust structural stress parameter for evaluation of multiaxial fatigue of weldments. *J. ASTM Int.* **2006**, *3*, 1–17. [CrossRef]
36. Zhao, W.Z.; Li, X.W.; Dong, P.S. *Anti-Fatigue Design Theory and Method of Welded Structure*; China Machine Press: Beijing, China, 2017.
37. Morais, G.; Martin, R.; Silva, J. Random vibration fatigue of welded structures—Applications in the automotive industry. *Procedia Struct. Integr.* **2019**, *19*, 175–193. [CrossRef]
38. Pei, X.; Ravi, S.; Dong, P.; Li, X.; Zhou, X. A multi-axial vibration fatigue evaluation procedure for welded structures in frequency domain. *Mech. Syst. Signal Pr.* **2022**, *167*, 108516. [CrossRef]
39. Zacher, M.; Nicklisch, D.; Grabner, G.; Polach, O.; Eickhoff, B. A multi-national survey of the contact geometry between wheels and rails. *Proc. Inst. Mech. Eng. Part F J. Rail Rapid Transit* **2015**, *229*, 691–709. [CrossRef]
40. Gialleonardo, E.D.; Facchinetti, A.; Bruni, S. Control of an integrated lateral and roll suspension for a high-speed railway vehicle. *Veh. Sys. Dyn.* **2023**, *61*, 472–498. [CrossRef]
41. Magel, E.; Kalousek, J. Designing and assessing wheel/rail profiles for improved rolling contact fatigue and wear performance. *Proc. Inst. Mech. Eng. F J. Rail Rapid Transit* **2017**, *231*, 805–818. [CrossRef]
42. Magel, E.; Kalousek, J. The application of contact mechanics to rail profile design and rail grinding. *Wear* **2002**, *253*, 308–316. [CrossRef]
43. Crosbee, D.; Allen, P. Development of a Tram-Train wheel profile for dual-operation running. In Proceedings of the 1st International IMechE Stephenson Conference, London, England, 21–23 April 2015; Available online: http://eprints.hud.ac.uk/id/eprint/27316/ (accessed on 25 June 2022).
44. Muhamedsalih, Y.; Tucker, G.; Stow, J. Optimisation of wheelset maintenance by using a reduced flange wear wheel profile. *Proc. Inst. Mech. Eng. F J. Rail Rapid Transit* **2023**, *237*, 253–265. [CrossRef]
45. Muhamedsalih, Y.; Stow, J.; Bevan, A. Use of railway wheel wear and damage prediction tools to improve maintenance efficiency through the use of economic tyre turning. *Proc. Inst. Mech. Eng. F J. Rail Rapid Transit* **2019**, *233*, 103–117. [CrossRef]
46. Temple, P.; Harmon, M.; Lewis, R.; Burstow, M.; Temple, B.; Jones, D. Optimisation of grease application to railway track. *Proc. Inst. Mech. Eng. F J. Rail Rapid Transit* **2017**, *232*, 1514–1527. [CrossRef]
47. Piao, M.; Yang, J.; Liu, D.; Fang, J.; Tian, D. Design defaults of German ICE3 serial bogies and technical solutions. *Computer Integr. Manuf. Syst.* **2016**, *22*, 1654–1669. [CrossRef]
48. Zhou, Q.Y.; Liu, F.S.; Zhang, Y.H.; Tian, C.; Yu, Z.; Zhang, J. Solutions for problems at wheel-rail interaction in high speed railway. *China Railw. Sci.* **2017**, *38*, 78–84. [CrossRef]
49. Piao, M.; Yang, J.; Zhao, Q.; Ding, Y.; Zhao, W. Rigid-flex coupling simulation singularity of high-speed rolling stocks and transaction strategy. *Comput. Integr. Manuf. Syst.* **2015**, *21*, 2456–2466. [CrossRef]
50. Piao, M.; Li, M.; Zhao, Q.; Zhao, W. Lateral vibration coupling mechanism of high-speed rolling stocks and damping technical countermeasure. *J. Vib. Shock.* **2015**, *34*, 83–92 and 107. [CrossRef]
51. Yang, J.; Piao, M.; Gao, W.; Fu, K.; Gao, H. Lateral vibration reduction technical strategy of high-speed pantograph based on wheel-rail and pantograph-catenary dual coupling interactions. *Comput. Integr. Manuf. Syst.* **2019**, *25*, 1908–1919. [CrossRef]
52. Li, T.; Piao, M.; Fan, J.; Fang, Z.; Li, G.; Jin, S. Dynamical design of self-adaptive high-speed bogies based on full-vehicle stability properties and variation patterns. *Comput. Integr. Manuf. Syst.* **2022**, *28*, 385–408. [CrossRef]
53. Li, T.; Du, W.; Piao, M.; Guo, Y.; Jin, S.; Nie, C.; Fang, J.; Cheng, Y.; Fan, J. Dynamical effect investigations of component's internal interface by using techniques of rigid-flex coupling simulation. *Shock Vib.* **2021**, 6509950. [CrossRef]

54. Tang, M.; Xiong, X.; Li, X.; Zhang, J.; Chen, G.; Wang, K. Vibration characteristics of outer windshield structures of high-speed trains based on fluid–structure interactions. *Nonlinear Dyn.* **2023**, *111*, 2111–2132. [CrossRef]
55. Wang, Q.; Piao, S.; Piao, M.; Dang, P.; Li, Q.; Ren, J. A dynamic design methodology for large-scale complex nonlinear dynamic systems based on orthogonal decomposition technique. *Shock Vib.* **2023**, 7152223. [CrossRef]

Disclaimer/Publisher's Note: The statements, opinions and data contained in all publications are solely those of the individual author(s) and contributor(s) and not of MDPI and/or the editor(s). MDPI and/or the editor(s) disclaim responsibility for any injury to people or property resulting from any ideas, methods, instructions or products referred to in the content.